

PROJECT COMPLETION REPORT
Report No: NML-GAP0088-03-2006
(Sanction Letter No. III.5(28)/99-ET dated 17/06/02)

Modelling of Crack-tip Blunting using Finite Element Method (FEM)

A research project funded by
Department of Science & Technology
Ministry of Science & Technology
Under SERC (Engineering Science) scheme

Ms. Mita Tarafder (PI)
Dr. Soumitra Tarafder (Co-PI)



National Metallurgical Laboratory
(Council of Scientific & Industrial Research)
Jamshedpur – 831007



National Metallurgical Laboratory

Jamshedpur-831007

PROJECT COMPLETION REPORT

Project Title: Modelling of crack tip blunting using Finite Element Method	Project No: GAP-0088
Project Team Mita Tarafder, Byomkesh Dash Swati Dey, S. Sivaprasad S.K. Das, S. Tarafder	Date of Project Initiation: 23 June 2002
	Date of Project Completion: 31 December 2006
	Project Cost: Rs. 16,55,204/- (DST: Rs. 11,04,136 and NML: Rs.5,51,068)
Customer/Client's name and address for externally funded projects Dr. V. Raghupathy, Scientist G, Department of Science and Technology Technology Bhavan, New Mehrauli Road, New Delhi-110016	Class: Public document (Free/Priced) Restricted Circulation/ Only to client/Secret
	Classification: Inhouse/Grant-in-aid/Sponsored/ Consultancy / Collaborative
	Date of Report: 31.03.06
Area: Engineering Science Sub Area: Computational Fracture Mechanics	Project Ref No: Sanction Letter No. III.5(28)/99-ET dated 17/06/02
	Specify Type: <input checked="" type="checkbox"/> Ongoing Area <input type="checkbox"/> New Area Initiated
Key words: Crack tip blunting, CTOD, fracture toughness, FEM, ductile material	
Abstract <p>For determination of fracture toughness in engineering structural materials, the standard procedure specifies the generation of a crack growth resistance curve (R curve) experimentally and identification of the critical toughness parameter by the intersection of an offset to a blunting line on the R curve. The use of a theoretical blunting line, as proposed in the standards, often gives conservative fracture toughness values particularly in high toughness materials. In this project, through finite element simulation of standard fracture mechanics test specimen, the crack blunting process in ductile materials is proposed to be investigated. From the load-displacement data generated by FEM, the crack tip opening displacement ($CTOD$) as well as J, an energy parameter of elastic plastic fracture mechanics, and Δa, the crack extension, accompanying the blunting process have been calculated. The effect of variation of material properties like Young's modulus, E, yield stress, σ_y and strain hardening parameter, n, on the shape and slope of the blunting line has been established. The numerically obtained blunting line has been validated using experimental results. Important conclusions drawn from this investigation are the following</p> <ul style="list-style-type: none">◆ the blunting line is mildly sensitive to the level of flow stress, with the inflection occurring at a lower flow stress and with reduced sharpness as the flow stress is increased. The blunting line slope is higher in low strength materials.◆ the nature of the blunting line is greatly dependent with the work hardening capacity of the material, with the overall slope of the blunting line increases with increased hardening behaviour.◆ the crack tip profile is elliptical not semicircular. For the low strain hardening materials the major axis is more than the minor axis i.e. $CTOD < 2 \cdot da$. In case of high strain hardening materials reverse co-relation is observed i.e. $CTOD > 2 \cdot da$.	
Report Issuance Authority: Name: Ms. Mita Tarafder Signature:	

- 1. Title of the project :** Modelling of crack tip blunting using Finite Element Method
- 2. Date of sanction :** 17 June 2002
- 3. Total amount sanctioned :** Rs. 16,55,204/-(DST: Rs. 11,04,136 and NML: Rs.5,51,068)
- 4. Total amount received :** Rs. 10,57, 494
- 5. Date of commencement of the project :** 23 June 2002
- 6. Date of completion of the project :** 31 December 2005
- 7. Original objectives :** The objectives of this project are
 - to investigate the blunting behaviour of crack tips in high toughness materials using finite element method (FEM).
 - to examine the effect of mechanical properties (E , σ_y and n) and specimen geometry on the blunting line slope
 - to validate the numerically obtained blunting line slopes with experimentally measured values
 - to explore the possibility of proposing a universal blunting line equation for a wide range of properties of engineering materials.
- 8. Modification in objectives, if any, during the course of the project with reasons thereof :** None
- 9. Details of actual work that could be accomplished with quantitative results achieved**

To attain the objectives of this project four major activities have been performed such as Finite Element (FE) Analysis, Experimental validation of FE results, On-line crack tip monitoring system and Special data analysis routines for experimental determination of blunting line. Quantitative results have been discussed in the forthcoming sections.

9.1 Finite Element Analysis

Finite Element (FE) Method has been used to model the crack tip profile of standard fracture mechanics specimen. Varying the material properties like Young's Modulus (E), Yield Strength(σ_{ys}) and Strain hardening coefficient(n), the crack tip profile parameter, X and the blunting line slope M have been computed. For generating numerical data we have carried out 32 analyses using the FE analysis package ABAQUS 6.4 [1]. Numerous engineering materials have been analyzed and the results were compared with the experimental data.

9.2 Experimental validation of FE results

Experimental investigation has been carried out to obtain crack growth resistance curves (J - R curves) for highly ductile materials by fracture toughness testing of metallic materials following the ASTM standard E1152 [2]. For this investigation High Strength Low Alloy Steel (HSLA), Line Pipe steel (TLXAL) and SA333 materials are chosen for their high toughness property.

9.3 On-line crack tip monitoring system

For on-line monitoring of the crack tip profile, a high resolution CCD camera based "Real-time optical crack tip monitoring system (ROMS)" has been designed and the set-up installed. Figure 1(a) shows the picture of the ROMS set-up being used for crack tip monitoring during fracture tests. ROMS set-up with CCD camera attached with the servohydraulic machine is shown in Figure 1(b).



Figure 1 (a) : ROMS set-up being used for crack tip monitoring



Figure 1 (b) : ROMS set-up with CCD camera attached with the servohydraulic machine

9.4 Special data analysis routines for experimental determination of blunting line

As a part of the work carried out in the project, a menu-driven software named *Fracture Data Analyser* (FracDA) has been developed in Visual C++ which can calculate various

parameters like load, displacement, crack tip opening displacement and simultaneously plots various graphs and also compares the data obtained from experimental data and FE analysis.

The user is required to input the data obtained from finite element analysis. The input data includes the time step, reaction force, crack mouth opening displacement (CMOD) and displacement due to virtual crack extension. The user is also required to input geometry specifications of the specimen and material properties, i.e. the Young's modulus, the Poisson's ratio and the yield stress. At present this software has the options to include geometry of two specimen types: three-point bend specimen and CT specimen. This software also has the capability to display various plots like load-displacement curve, CTOD and J -integral values with respect to the extension of crack length from FE data and compare them with the same generated from experimental data.

The software carries out a large amount of calculations, taking the voluminous data generated through FEM as input, and thus serves as a useful tool for evaluating the FEM data vis-à-vis that generated experimentally. Thus, it can validate and verify the FE data immediately after performing the FE analysis.

Detailed discussion on the methodology adopted and results obtained is given below.

10. Detailed analysis and discussion of the results

When a sharp pre-crack contained in a high toughness material is loaded, the event occurring at the crack tip follows a sequence which can be itemized as

1. Crack tip blunting
2. Crack initiation
3. Stable tearing
4. Unstable crack growth

Upon development of intense stress and strain fields at the tip of the pre-crack on loading, the crack tip blunts under the influence of the tensile pull created by the surrounding material. The blunting of the pre-crack is accompanied by virtual extension of the crack with respect to the original position of the tip due to Poisson's contraction, and a characteristic crack tip opening displacement (CTOD). On continuation of loading, a cracking initiates from the blunted pre-crack through ductile tearing. Stable

extension of the crack takes place subsequently, and in load controlled systems may be followed by unstable crack growth.

The above sequence of event of crack growth can be represented quantitatively by the J - R curve obtained by fracture toughness testing of metallic materials as per the ASTM standard E1152 [2]. Figure 2 shows a typical J - R curve indicating the initial linear blunting line, the initiation fracture toughness J_i and the stable tearing curve.

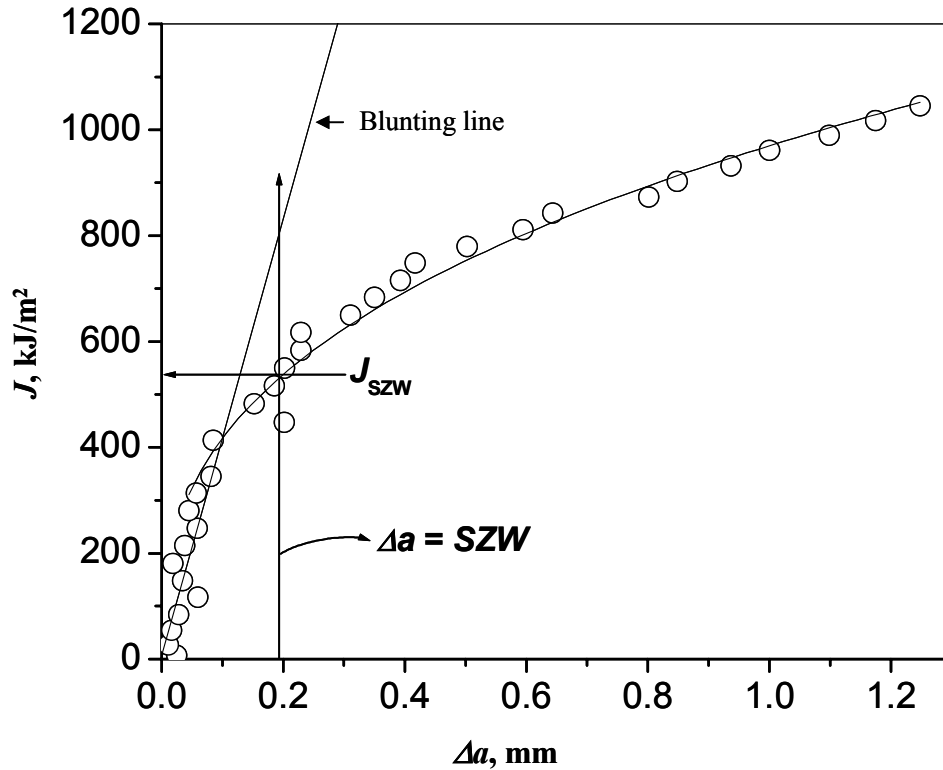


Figure 2: A typical J - R curve indicating the initial linear blunting line and the stable crack growth line

The blunting of a crack can be represented by the initial linear part of the J - Δa , R curve, which can be written as

$$J = M. \sigma_0 \Delta a \quad \dots \text{eq1}$$

where σ_0 the flow stress, M is the slope of the initial linear part of the J - Δa curve.

Here $M=X*Y$, where X is the slope of the linear part of the δ - Δa curve given as

$$\delta = X. \Delta a \quad \dots \text{eq2}$$

In Eq 2, δ is the crack tip opening displacement (CTOD). In the product form of $M = X \cdot Y$, Y is a constant originating from the relationship between J and δ

$$J = Y \sigma_0 \delta \quad \dots \text{eq3}$$

For simplicity, M is assumed as 2 [4] signifying a semicircular crack tip profile as shown in Figure 2 (a). It is argued that during crack growth, the semicircular profile can not be maintained especially in high toughness and high strength materials. The crack tip profile will be semi-elliptical as in Figure 2 (b). The aspect ratio between the major axis and the minor axis of the ellipse will determine the value of M .

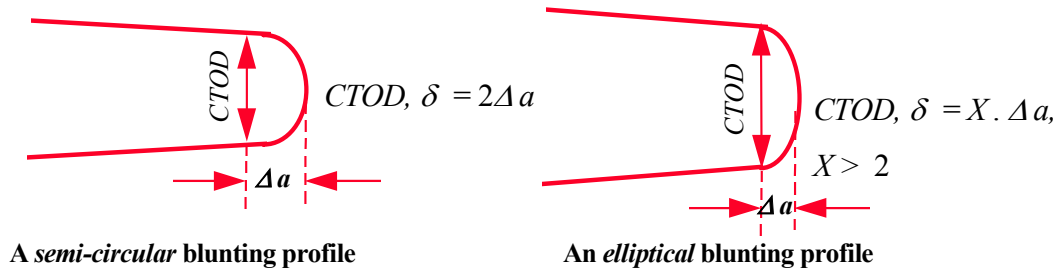


Figure 2: (a) Semi circular and (b) elliptical crack tip profiles

10.1 Finite Element Analysis

For the Finite Element (FE) analysis, standard fracture mechanics specimen geometry (three point bend-3PB) is modelled using the FEM software package ABAQUS. The schematic of the TPB specimen with loading configuration is shown in Figure 3. Here the span, half of the span (S) is double of the width of the specimen. The geometric dimension and the material property used in the FE analyses are given in appendix-I.

Taking advantage of the symmetry of the geometry about the crack planes, half of the specimen has been modelled. For FE meshing, eight node biquadratic plane strain quadrilateral, reduced integration element has been selected. Automatic meshing facility of ABAQUS has been used for meshing. Boundary condition for defining the fixity at the boundary nodes are shown in Figure 4.

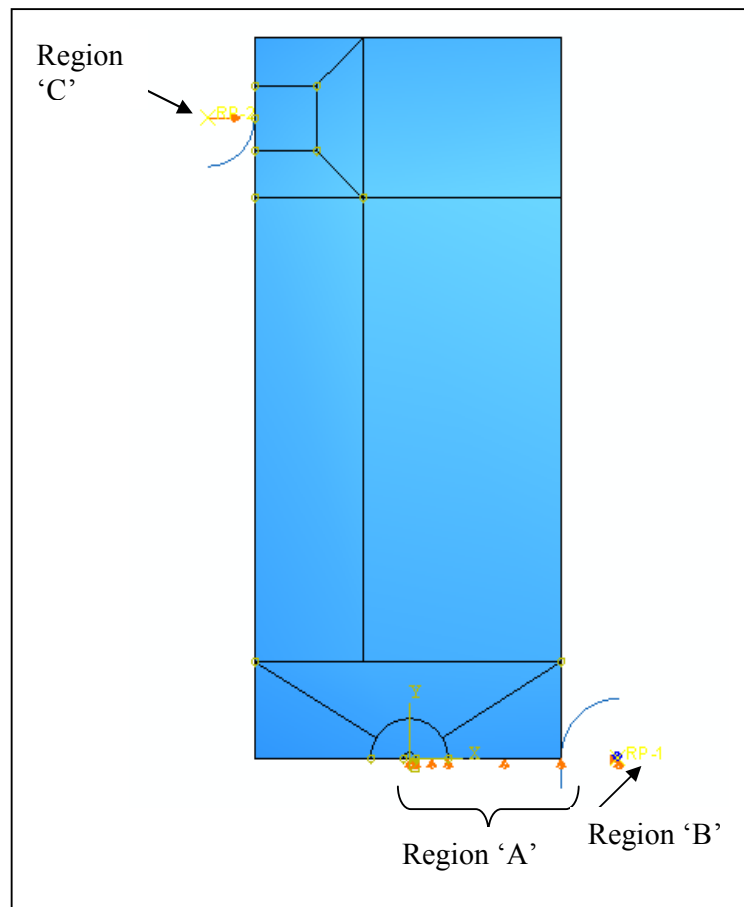
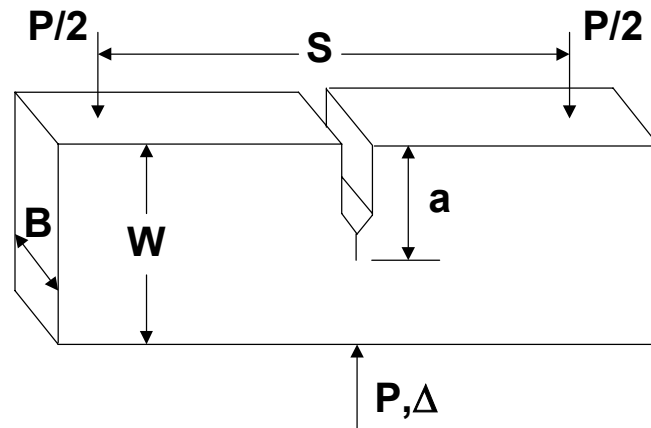


Figure 4: Three point bend specimen showing the boundary conditions

Region A: Here displacement in the y-direction is zero

Region B: Here displacement in the x-direction and y-direction is zero.

Region C: Here a displacement of 5mm is given in the x-direction.

Figure 5(a) shows the FE mesh and figure 5(b) highlights the finer mesh around the crack tip. It may be noted that the mesh near the crack tip is finer than the remaining part of the geometry. A crack tip root radius of 20 micron has been considered to carry out finite strain FE analysis. The FE mesh has 6554 nodes and 2125 elements.

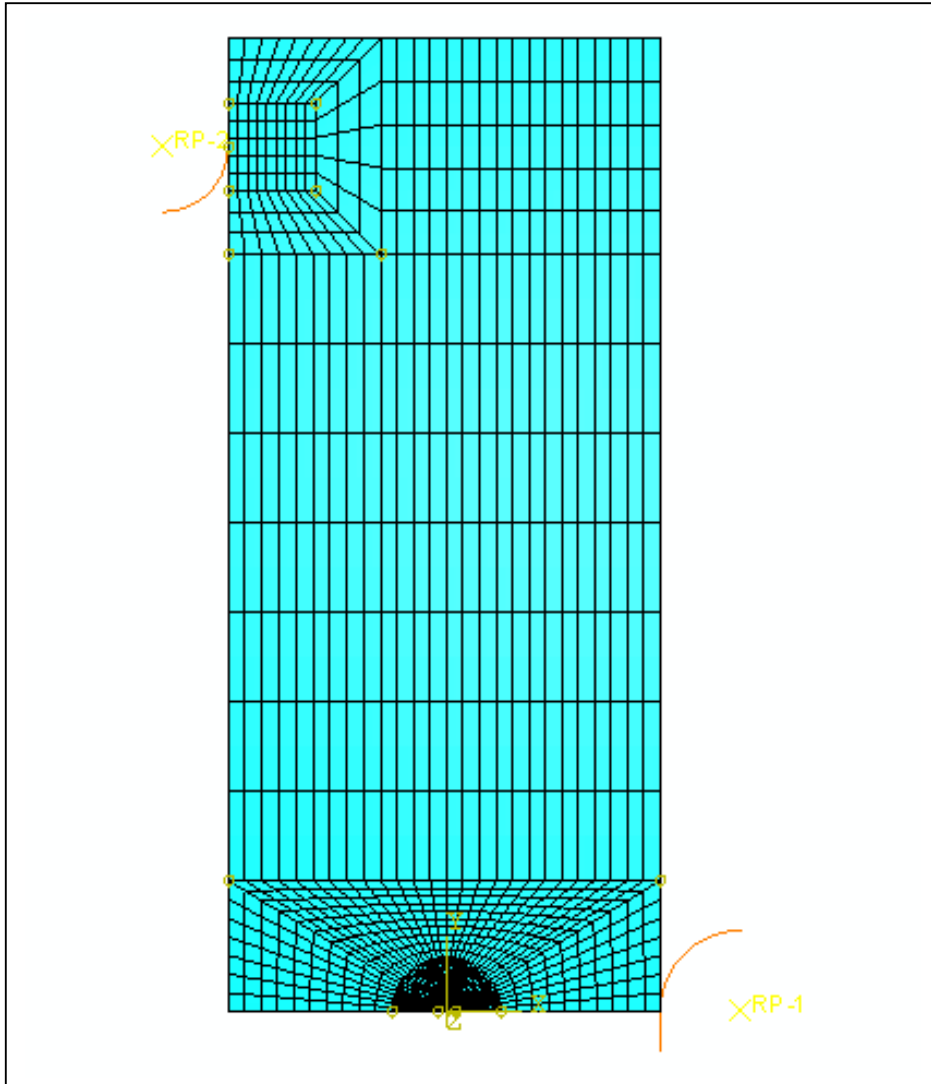


Figure 5 (a): Mesh diagram of three point bend specimen

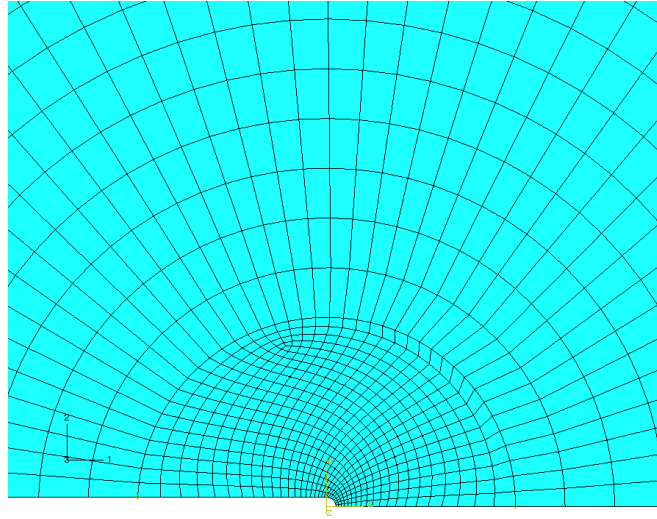


Figure 5 (b) : Mesh at the crack tip region specimen

10.1.1 Finite Element Mesh Optimisation

In FE formulation, a set of linear simultaneous equations are generated based on the principle of minimization of potential energy [3]. The total potential energy, Π of a deformable structure is obtained by adding the internal energy, U and the work potential WP as-

$$\begin{aligned} \Pi &= U + WP \\ \Pi &= \frac{1}{2} \int_V \sigma^T \epsilon dV - \int_V u^T f dV - \int_s u^T T dS - \sum_i u_i^T P_i \end{aligned} \quad \dots \text{eq 5}$$

Where $u^T = \{u_1, u_2, \dots, u_N\}$, $N = \text{no of FE nodes}$
 $\sigma^T = \{\sigma_x, \sigma_y, \sigma_z, \tau_{xy}, \tau_{yz}, \tau_{zx}\}$

At equilibrium, $\left. \frac{\partial \Pi}{\partial u_i} \right|_{i=1 \text{ to } N} = 0$ generates a set of simultaneous equations which can be expressed as

$$[K]\{u\} = \{F\} \quad \dots \text{eq 6}$$

Where $[K]$ is the global stiffness matrix generated by assembling a large number of element stiffness matrices and $\{F\}$ is the force vectors, $\{u\}$ is the displacement vector and $\{\sigma\}$ is the stress vectors. The element stiffness matrix is formulated on the basis of strain-displacement correlation matrices, $[B]$ and $[A]$ of the element and the material stiffness matrix, $[D]$.

Thus the element stiffness matrix, K_e can be given as-

$$\text{Element stiffness matrix, } K_e = t_e \cdot [A] \cdot [B^T] \cdot [D] \cdot [B] \quad \dots \text{eq 7}$$

where t_e = the thickness of the element

A = the strain-displacement matrix in local co-ordinate system

B = the strain-displacement matrix in global co-ordinate system

D = the material stiffness matrix.

It may be noted from Eq 7 that changes in K_e is due to the variations of A, B and D matrices and the thickness of the element. Any change in FE mesh will alter the A and B matrices whereas the change in materials will modify D matrix. To study the variation of material property on the deformation behaviour of materials, it is required to generate FE data invariant to the mesh. For generating reliable numerical data, therefore, the FE mesh needs to be optimized for the given specimen geometry. In this investigation, the optimization is performed for three types of meshes: Coarse, Medium and Fine depending upon the mesh density near the crack tip. For meshing the crack tip area approximately 200, 400 and 800 elements were used. The FE results for these three mesh sizes are presented as load displacement plots in Figure 6. Since very little deviation is found in the load-displacement plot, we have considered the Medium mesh for all the analyses.

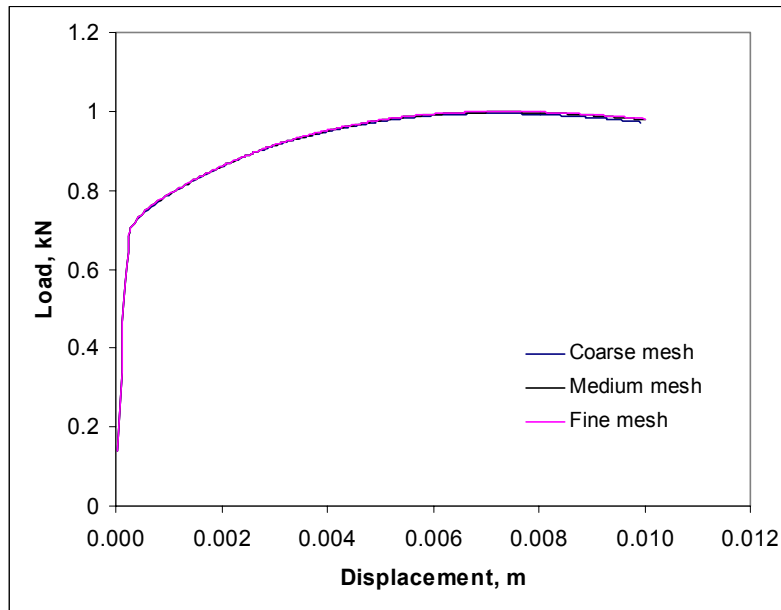


Figure 6: Load-displacement plots generated for coarse, standard and fine meshes showing very little deviation.

Using ABAQUS software packages, elastic-plastic FE analyses have been performed for analyzing TPB specimen geometry considering HSLA, TLXAL and SA333 materials. For validation of FE results in elastic-plastic case, we have used load-

displacement data obtained by experiments conducted as per the ASTM E1173 [4] standard on *Standard Test Method for J Integral Characterisation of Fracture Toughness*. Figures 7 (a, b and c) indicate the agreement between the FE results and the experimental data for the HSLA, TLXAL and SA333 materials in the linear and blunting regions. Since in the FE model, the crack growth has not been simulated, the FE results do not show any loss of stiffness and the load-displacement curve by FE shows always an increasing trend. In practical situation, as the crack propagates, the geometry loses its stiffness, and after reaching a maximum limit, unstable fracture occurs causing the abrupt falling of the load-displacement curve.

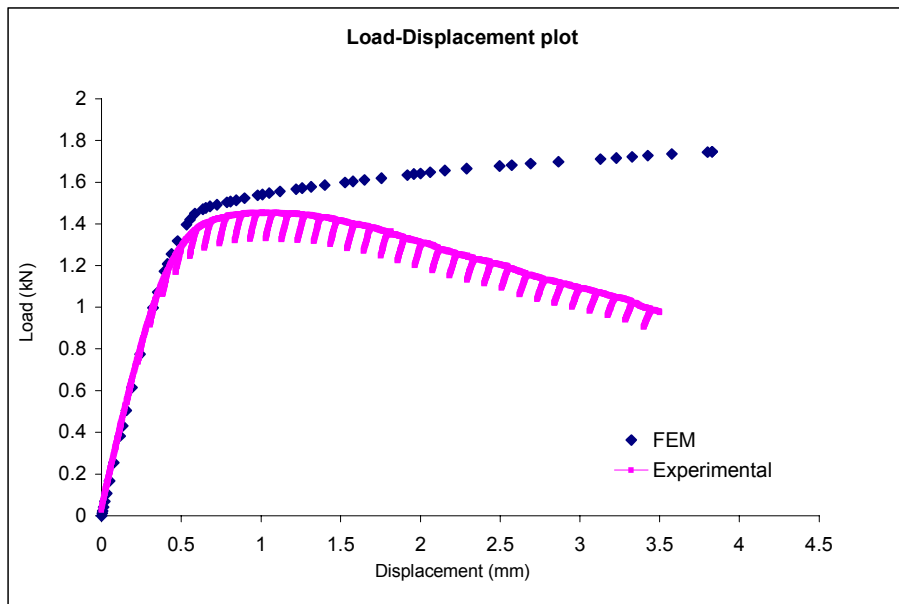


Figure 7 (a): Load-displacement plots for the HSLA-100 material

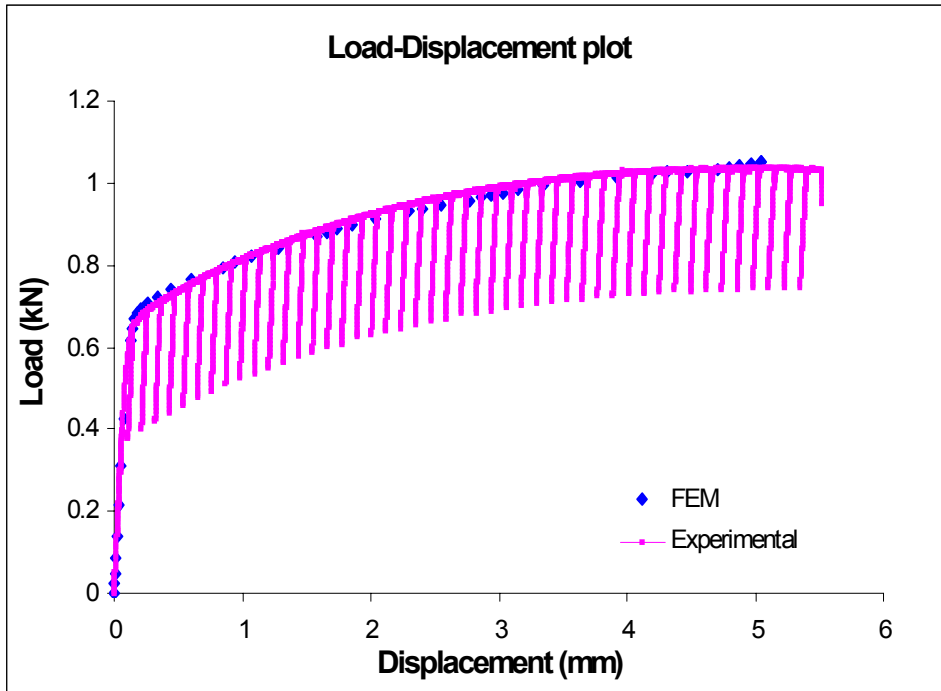


Figure 7 (b): Load-displacement plots for the SA333 material

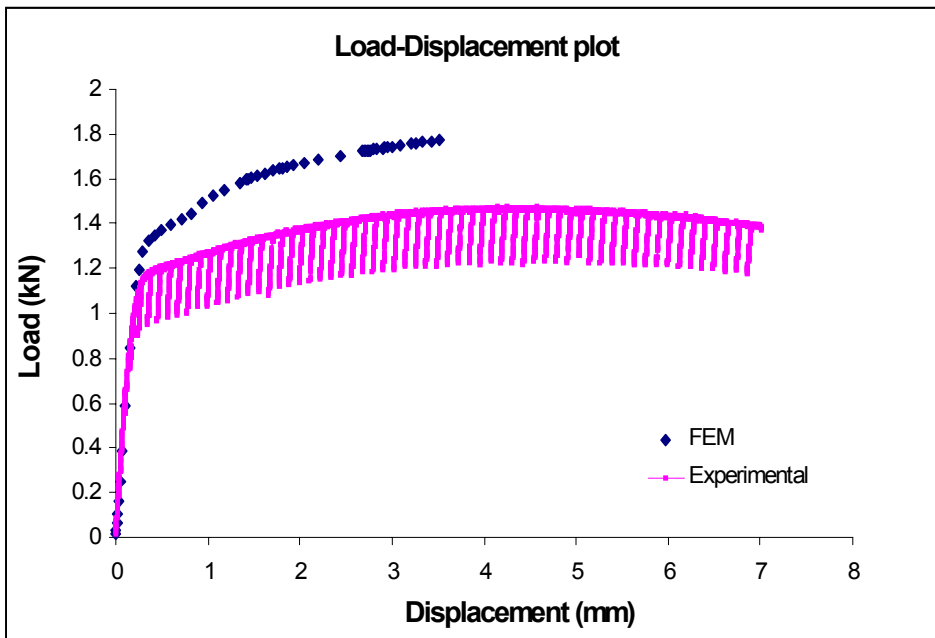


Figure 7 (b): Load-displacement plots for the Line Pipe steel, TLXAL material

10.1.2 Finite Element Test Matrix

The FE test matrix was designed to model a wide range of materials by varying material properties like Young's modulus (for differentiating steel and aluminum), Yield stresses (brittleness and ductility) and strain hardening coefficient (toughness property).

Some analyses code N334, N335, N304, N305, N314, N315, N324 and N325 given in the Table 1 can hardly be found in practical materials. However for understanding materials with properties at extreme boundaries, the analyses have been carried out.

10.1.3 Finite Element Results

To model crack tip blunting phenomenon by FE analysis, three fracture parameters such as J integral, Δa and CTOD have been computed using the numerical results.

Two methods have been used while computing J –integral using FE simulation [5]. The first method is similar to the technique being usually employed for computing J from the experimental load-displacement data. For estimating J from the FE simulation, the formulation used is given as

$$J = \frac{1}{B} \left(\frac{dW}{da} \right) \quad \dots \text{eq 8}$$

where W is the strain energy density which is the area under the load-displacement curve, da is the crack extension and B is the thickness of the specimen.

In the second method, contour integral [6] has been employed in which strain energy is calculated from the specified contours surrounding the crack tip in the FE model. The formulation used for computing J using the contour integral method is given as

$$J = \int_{\Gamma} \left(W dy - T \frac{\partial u}{\partial x} ds \right) \quad \dots \text{eq 9}$$

where Γ is a closed contour followed counter clockwise in a stressed specimen, T is the tension vector (traction) perpendicular to Γ in the outside direction, u is the displacement in the x-direction and ds is an element of Γ .

The procedure employed for computing crack extension, da , from the FE results has been highlighted in appendix-II.

For estimating CTOD from the FE simulation, standard ASTM procedure considering crack mouth opening displacement has been used. The detailed discussion on this has been included in appendix-III.

Figures 8, 9 and 10 show the J - da and CTOD- da plots for HSLA-100, SA333 and Line pipe steel materials.

Table 1: Test Matrix for Finite Element Analysis

#	<i>Test ID</i>	<i>E (GPa)</i>	σ_{ys} (MPa)	<i>n</i>
1.	E030	50	1000	0
2.	E130	100	1000	0
3.	E230	150	1000	0
4.	E330	200	1000	0
5.	S300	200	100	0
6.	S310	200	300	0
7.	S320	200	600	0
8.	S330	200	1000	0
9.	N330	200	1000	0
10.	N331	200	1000	0.1
11.	N332	200	1000	0.2
12.	N333	200	1000	0.3
13.	N334	200	1000	0.6
14.	N335	200	1000	1
15.	N300	200	100	0
16.	N301	200	100	0.1
17.	N302	200	100	0.2
18.	N303	200	100	0.3
19.	N304	200	100	0.6
20.	N305	200	100	1
21.	N310	200	300	0
22.	N311	200	300	0.1
23.	N312	200	300	0.2
24.	N313	200	300	0.3
25.	N314	200	300	0.6
26.	N315	200	300	1
27.	N320	200	600	0
28.	N321	200	600	0.1
29.	N322	200	600	0.2
30.	N323	200	600	0.3
31.	N324	200	600	0.6
32.	N325	200	600	1

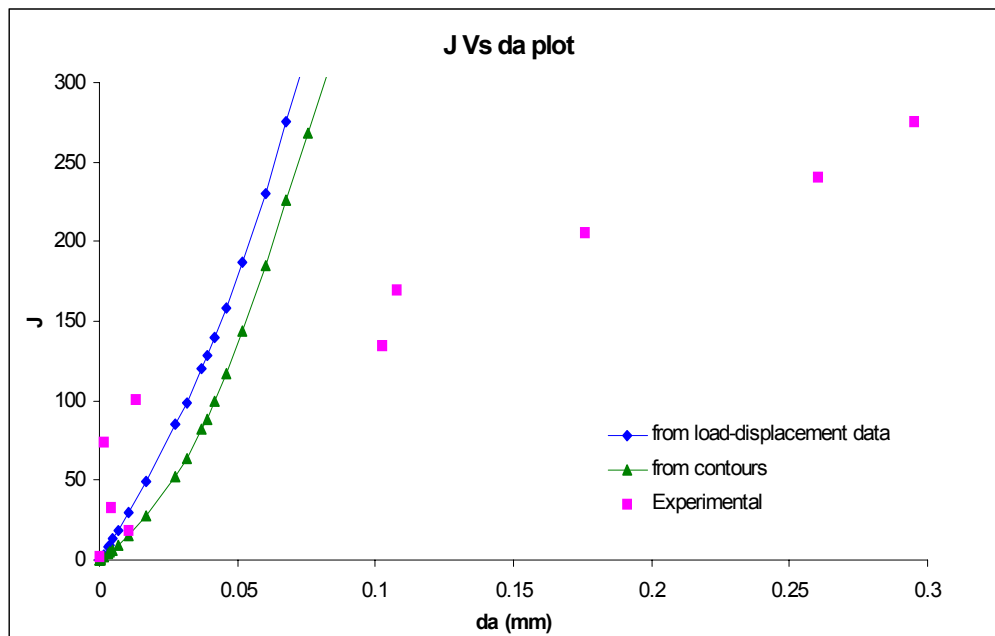
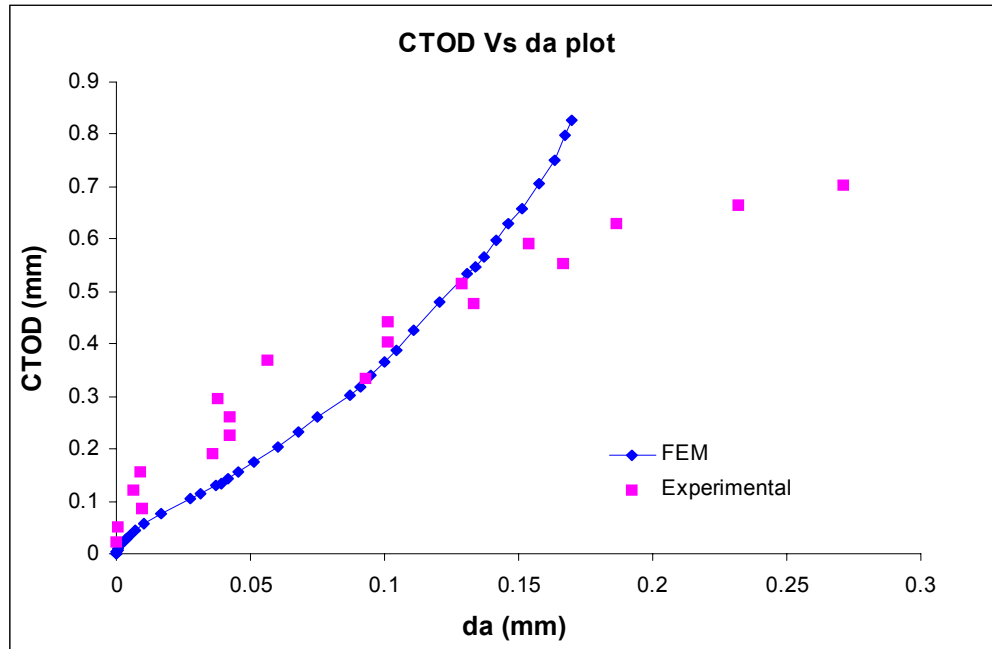


Figure 8: Variations of CTOD and J with da obtained by FE method and experimentally for HSLA-100 steel

The comparisons in the plots above show that the FE simulation reflects to a good approximation the situation observed experimentally.

Note that in the load-displacement plot as shown in figure 7, the FE data matches with the experimental data only to that extent up to which it may be expected that no real crack

extension takes place. Ductile tearing (real crack extension) has not been simulated using FEM since the objective of this project is to study the blunting behaviour of the crack that occurs prior to the real crack extension. The match observed between the data obtained from the FE analysis and the experimental data in the R -curve plots (CTOD vs Δa and J vs Δa plots) is considered to be sufficiently acceptable since the accuracy available in the experimental determination of Δa results in considerable scatter. In fact the FE data appears to follow a trend that matches that of the experimental data quite closely. The match of course is limited to the point at which ductile crack extension may be expected to occur.

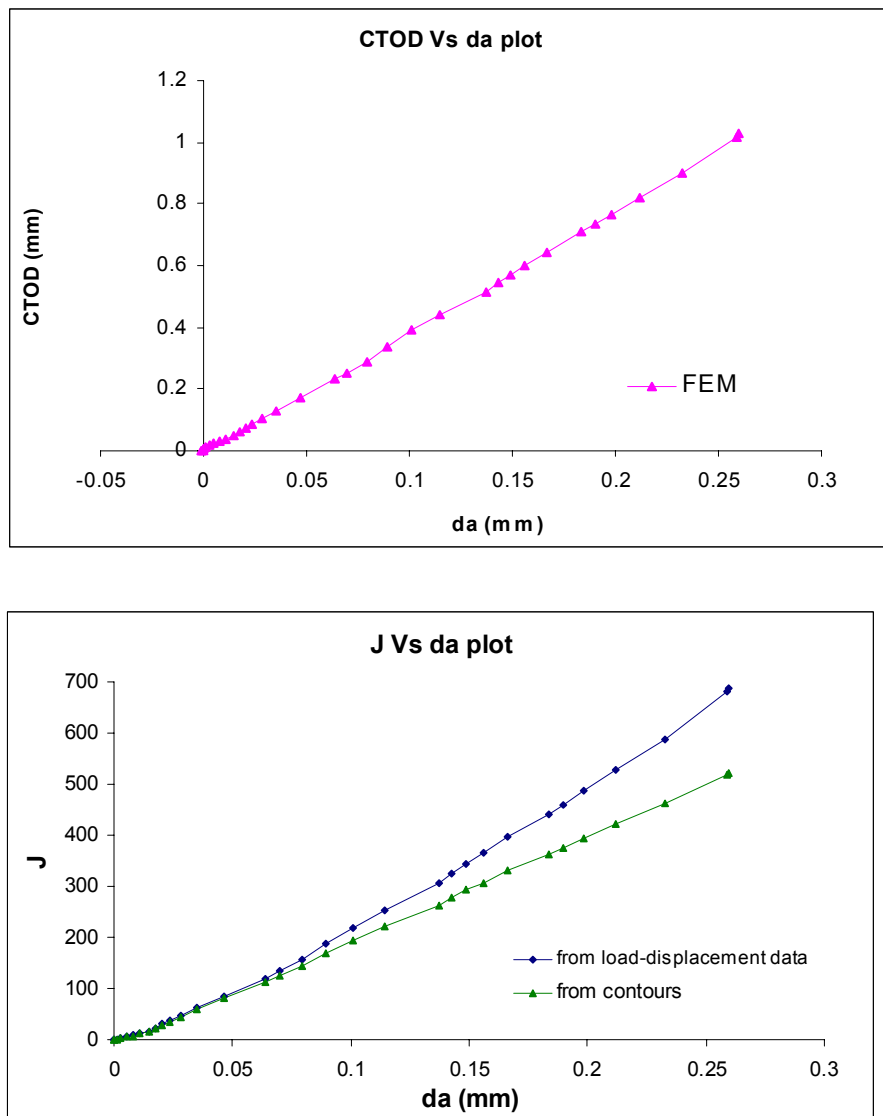


Figure 9: Variations of CTOD and J with da obtained by FE method and experimentally for SA 333 steel

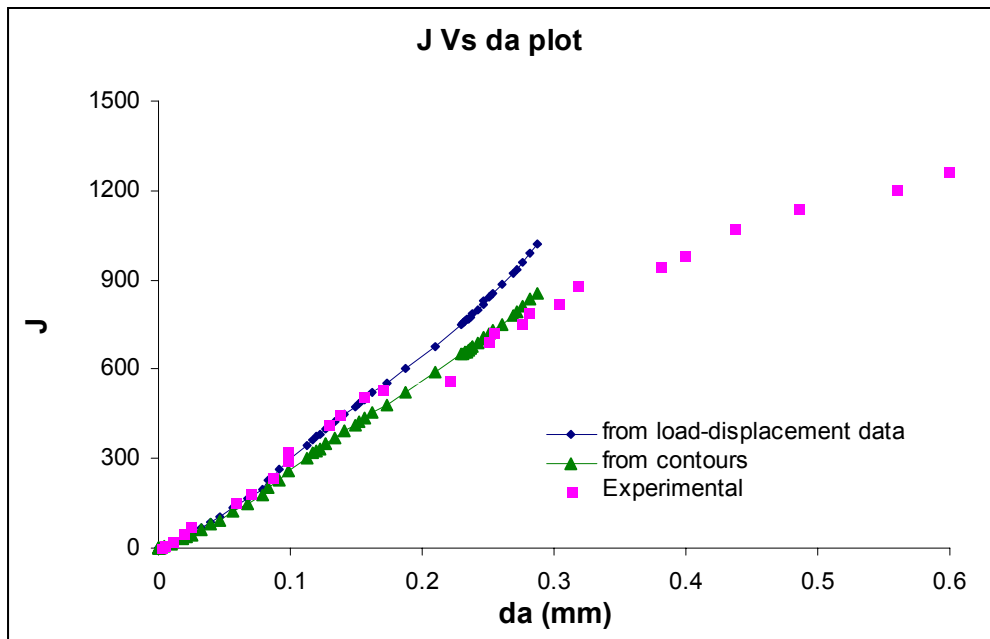
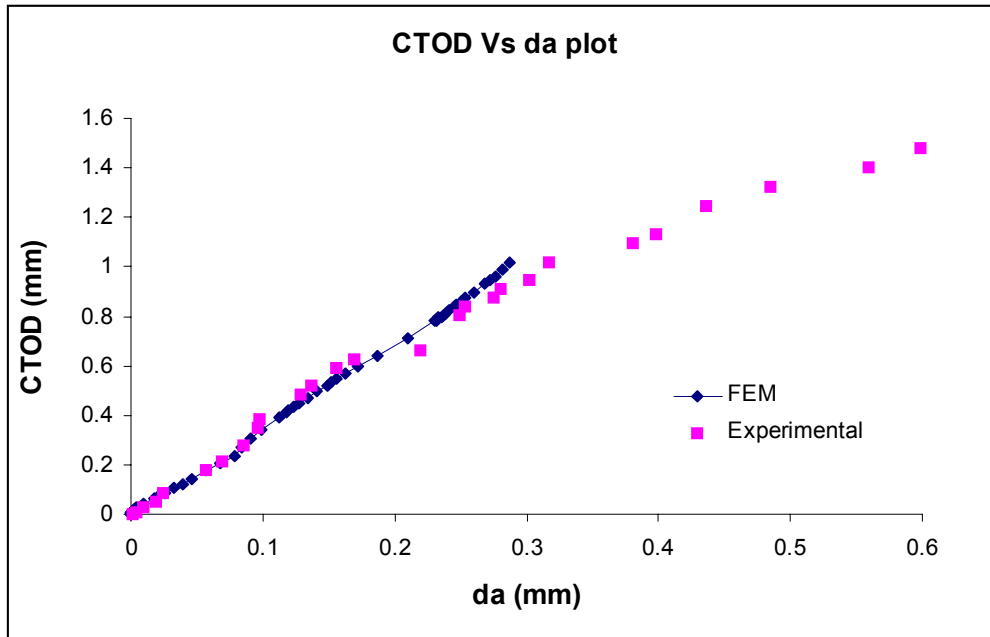


Figure 10: Variations of CTOD and J with da obtained by FE method and experimentally for Line Pipe steel

The comparison in the load displacement plots for the SA333 materials shows an excellent agreement between experimental and FE results. This is possible because the crack extension was delayed and the ductile tearing had not taken place till the presented data

range of the crack mouth displacement. Experimental data for the CTOD vs. da and J vs. da was not available and therefore comparisons could not be presented.

For the TLXAL or the Line Pipe materials, the agreement of the load displacement data obtained by experimental and FE methods is confined within the initial portion of the curves. Good agreement is found in CTOD vs. da and J vs. da results.

10.1.4 Modelling of the blunting line

To model the blunting line we need to compute δ i.e. the CTOD, da , the virtual crack extension and the J-integral values. Equations for studying the blunting line for materials can be given in the following forms-

$$\begin{aligned}\delta &= X \cdot \Delta a \\ J &= Y \sigma_0 \delta \\ J &= M \sigma_0 \Delta a, \text{ where } M=X \cdot Y\end{aligned}$$

The functional forms to represent X , the crack tip profile parameter, Y , the constant in the J - δ curve and M the blunting line slope can be given as-

$$\begin{aligned}X &= f(E, \sigma_{ys}, n) \\ Y &= g(E, \sigma_{ys}, n) \\ M &= h(E, \sigma_{ys}, n)\end{aligned}$$

It is required to assess the effect of each variable keeping others constant. Keeping σ_{ys} and n constant X , Y and M plotted with respect to E are given in figures 11 (a, b and c).

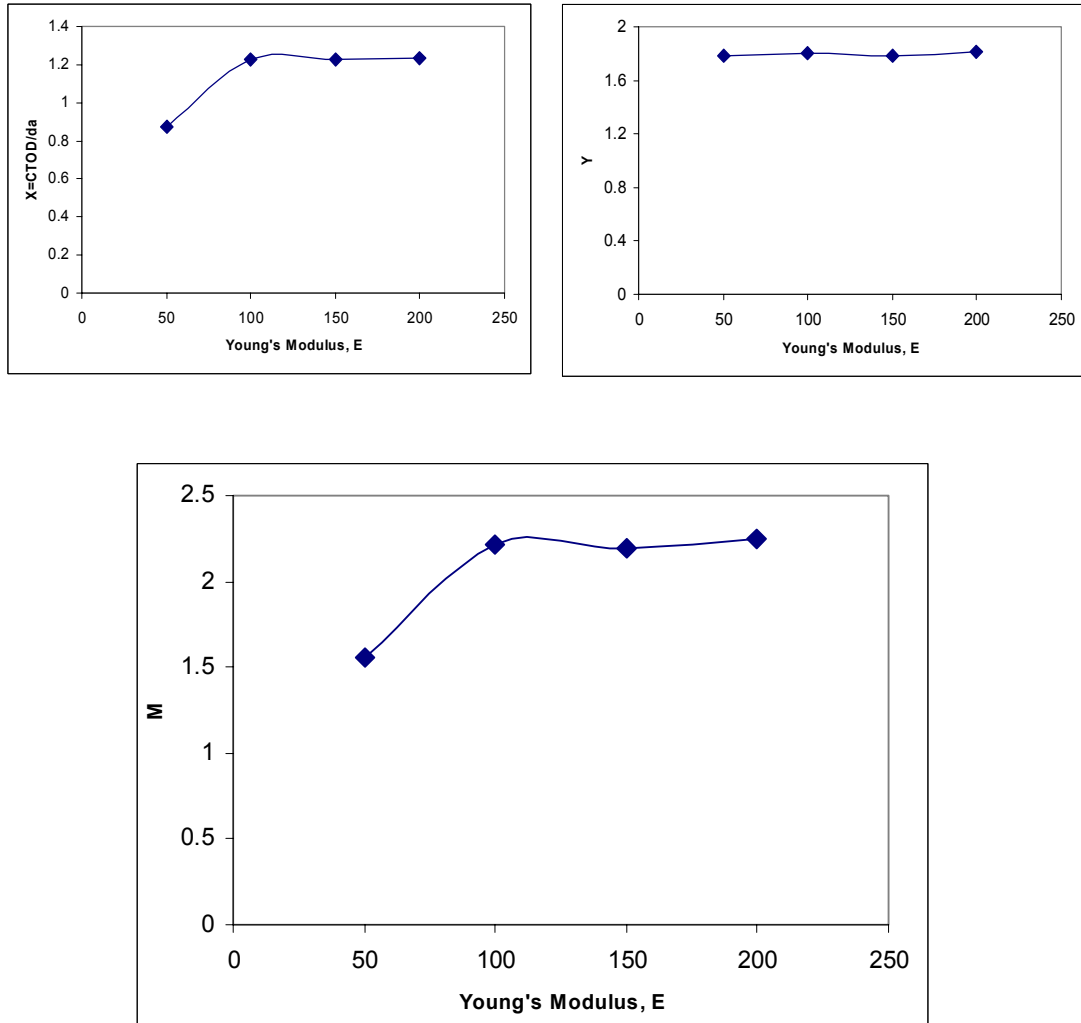


Figure 11 (a, b and c): Variations of X, Y and M with respect to the Young's Modulus(E) obtained from FE analyses

It can be seen that barring very low stiffness value, X , Y and M do not vary substantially. Since the materials investigated are primarily structural steels having stiffness within the range of 180 GPa to 220 GPa, we have considered the stiffness of 200 GPa for all the cases. Thus the functional formulation is modified further as

$$\begin{aligned}
 X &= f(\sigma_{ys}, n) \\
 Y &= g_I(\sigma_{ys}, n) \\
 M &= h_I(\sigma_{ys}, n)
 \end{aligned}$$

Figures 12 (a, b and c) show the variations of X , Y and M with respect to the strain hardening exponent for different σ_{ys} values.

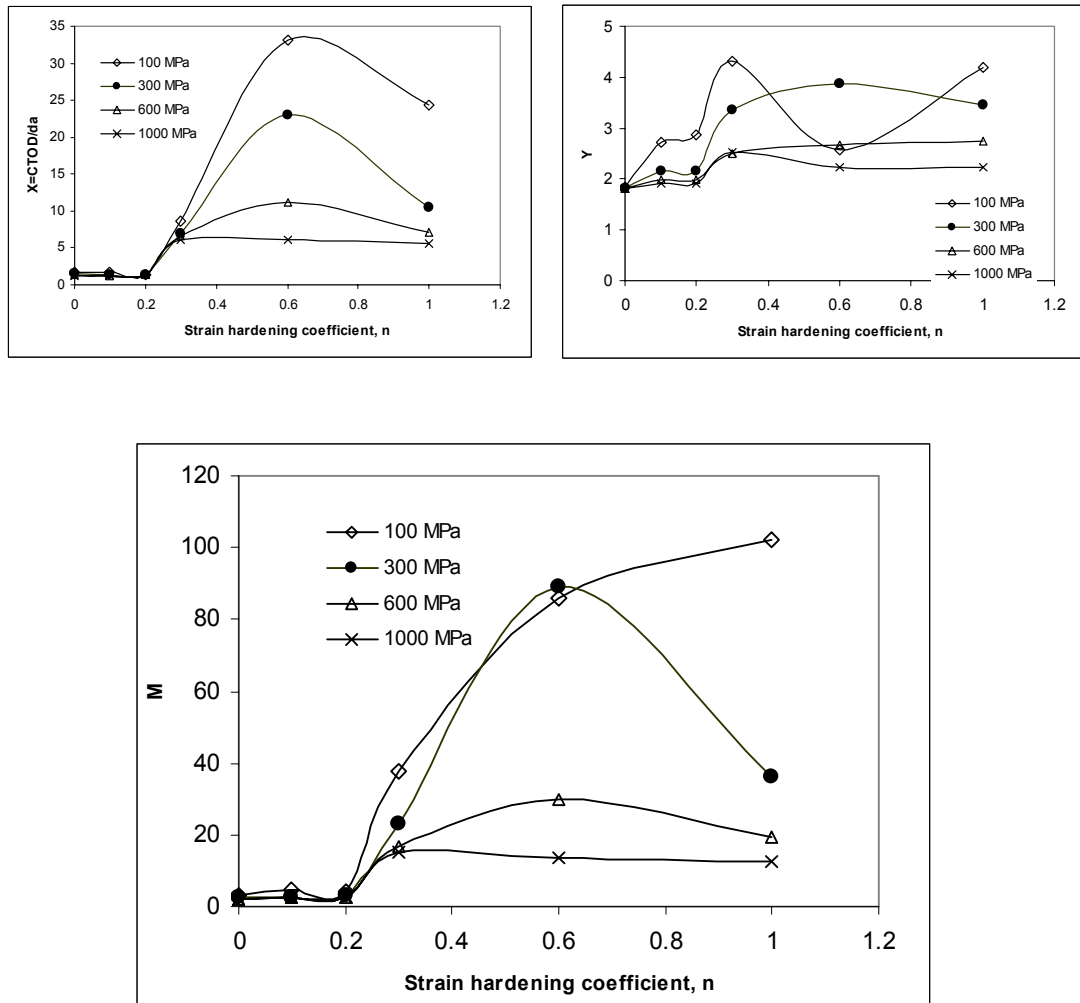
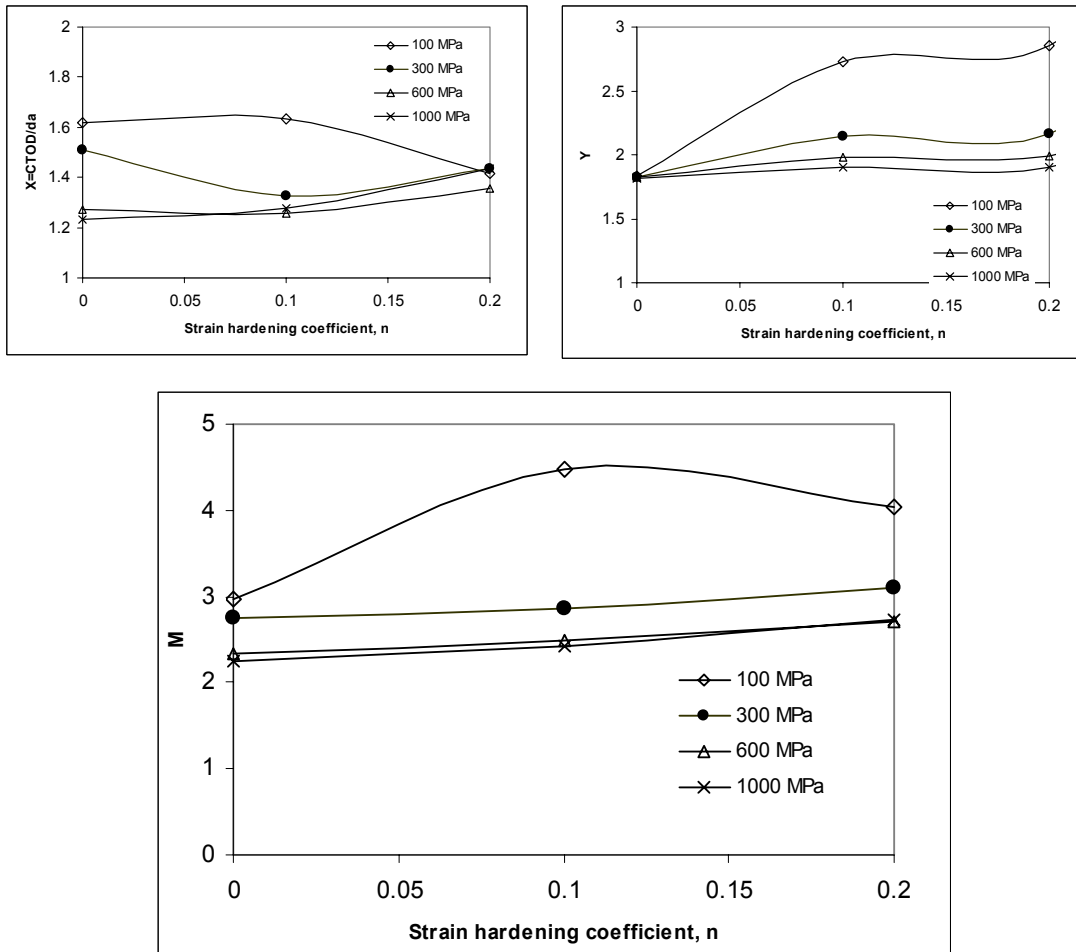


Figure 12 (a, b and c): Variations of X , Y and M with respect to the strain hardening coefficients obtained from FE analyses

For studying blunting behaviour, we need to investigate ductile materials having high toughness property. This is found in materials with very low strain hardening exponent, n [5]. Hence the range of n specifying the low strain hardening exponent is 0 to 0.2. Variations of X , Y and M for the range of n within 0 and 0.2 is given in figures 13 (a, b and c).



Figures 13 (a, b and c): Variations of X, Y and M with respect to the strain hardening coefficients within $0 < n < 0.2$ obtained from FE analyses

Variations of X, Y and M with respect to the yield stresses are plotted in Figures 13 (a, b and c) for the strain hardening coefficients 0-0.2 and in figures 14 (a, b and c) for 0.3-0.1.

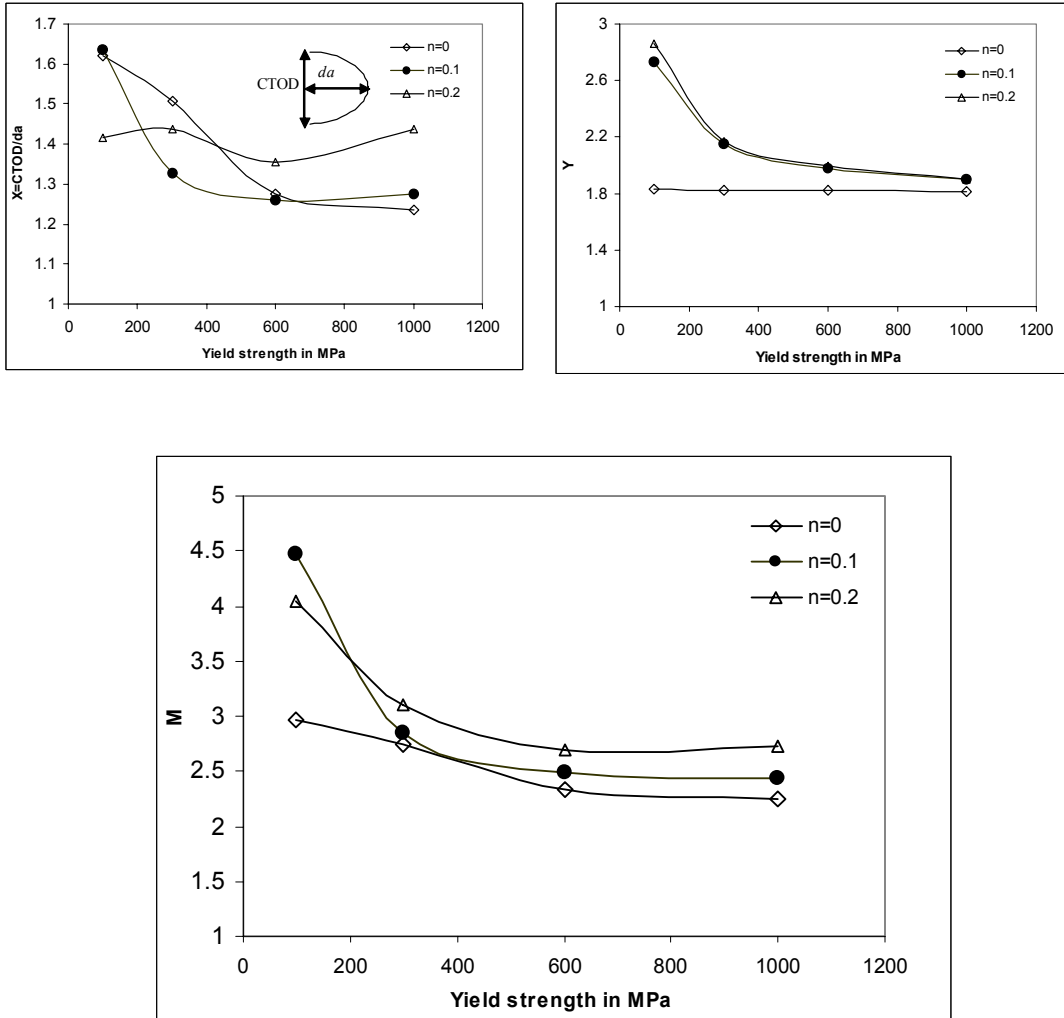
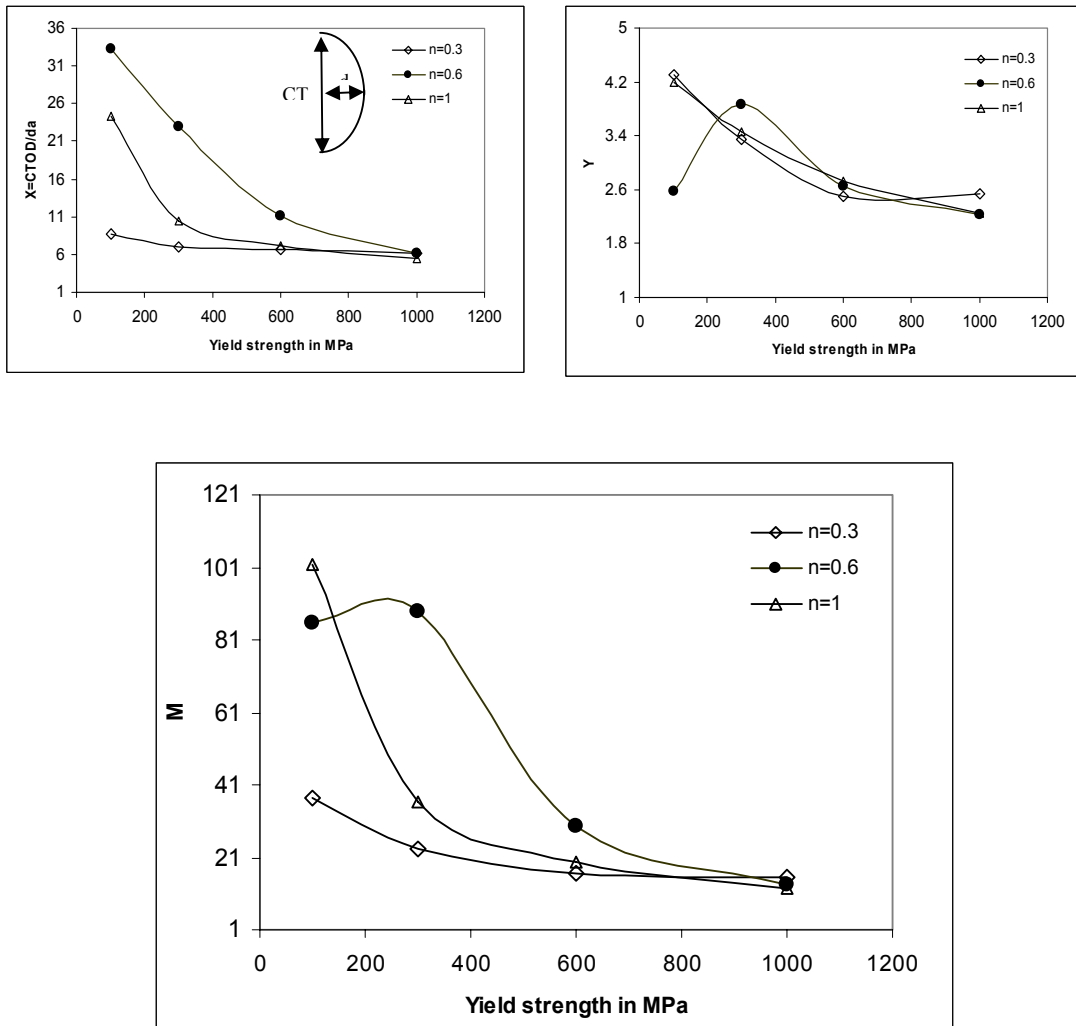


Figure 14: Variation of (a) X, (b) Y and (c) M w.r.t. yield strength for $n=0, 0.1$ and 0.2 obtained from FE analyses

Materials with low yield strength and high strain hardening behaviour tend to have high crack tip blunting. This extensive blunting makes the crack tip profile elliptical. In case of low strain hardening materials ($n=0$ to 0.2), the major axis is along the direction of the crack propagation whereas for high strain hardening materials ($n=0.3$ to 1) it is perpendicular to the same. It can be seen in figure 14 (a) that for $n=0$ to 0.2 , da is more than half of the CTOD. The proportionality of CTOD and da expressed by the crack tip profile parameter X is less than 2 for low strain hardening materials whereas it more than 2 in high strain hardening materials.



Figures 15: Variation w.r.t. yield strength for (a) X, (b) Y and (c) M for n=0.3, 0.6 and 1 obtained from FE analyses

Table 3 highlights the blunting line slope, M , obtained by experimental J - da curves for different structural materials. The same have been predicted using the plots in figure 3(c). In some cases, the experimental blunting line slopes do not agree with the predicted value obtained by FEM. The deviation may be the effect of plane strain condition of the specimen assumed for the FE analysis whereas the specimens did not meet the plane strain condition. It may further be pointed out that for representing material property we have used power law formulation which may be oversimplification as some of the high toughness materials show yield point elongation. Power law fitting of the non linear portion of the stress strain curve do not represent such elongation. Therefore for some of the grade of the HSLA steels, the blunting line slopes obtained by FEM underestimated the experimental values (see appendix-I for results).

Table 2: Blunting line slopes obtained by FEM and from experimental J - da curve

Materials	σ_{ys}	n	M_FEM	M_exp
HSLA-100_a	886	0.06	2.16	2.3
HSLA-100_b	831	0.08	2.4	2.2
HSLA-100_c	640	0.14	2.4	1.4
HSLA-100_d	927	0.16	2.4	1.4
HSLA-100-e	598	0.19	2.6	1.6
304LN	350	0.25	12	11.6
Line Pipe Steel	500	0.15	2.6	4.2

In our attempt to devise a universal blunting line equation to represent a wide range of materials, we have observed that the data obtained for M have exponential form. Systematic variation of data is not maintained especially for $n=0.1$ and $n=0.6$. It is difficult to estimate whether the deviation from the systematic trend is due to numerical error or the true consequence of material behaviour. We therefore suggest that the plots in figures 14 and 15 can be utilized for the prediction of the blunting line slopes for materials within the specified data range.

10.2 Determination of the crack tip profile

Crack tip profile can be estimated indirectly through fractographic measurement of stretch zone dimensions. The stretch zone (SZ) formed due to the excessive blunting of the crack tip in ductile materials prior to the onset of crack growth, will normally have two components: the stretch zone width (SZW) and the stretch zone depth (SZD). Figure 16 shows a schematic of the crack tip blunting process in ductile materials in which the virtual crack extension, Δa , represents the SZW and crack tip opening displacement, δ , corresponds to twice the SZD. If the crack tip profile is considered to be semicircular, SZW will be equal to SZD.

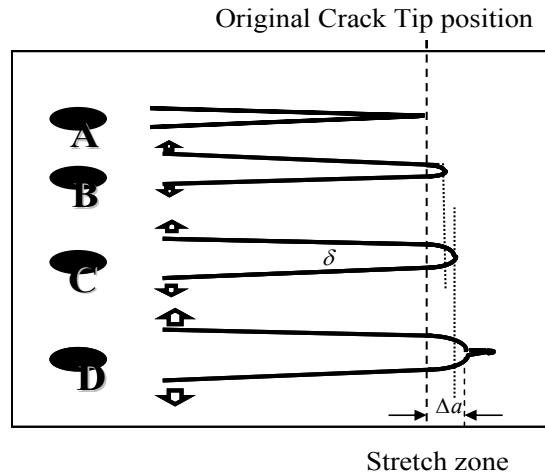


Figure 16: Various stages of crack extension in a ductile material

During crack tip blunting, a feature-less region, called stretch zone is created on the fracture surface which can be measured directly from the fractographs obtained by the scanning electron microscope (SEM). The distinct stretch zone can be measured manually or by using digital image processing techniques. In manual method a series of parallel lines are drawn throughout the fractographs, the edges of the stretch zone are marked and then the SZW is measured manually along these parallel lines. The average value of all these measurements is taken as the width of the stretch zone. The manual measurement of the SZW is time-consuming and tedious. Moreover, manual identification of the stretch zone boundaries is subjective and liable to large scatter in data. Errors generated by the manual measurements may lead to inaccurate interpretation of experimental results.

In this project a fully automatic method to measure the SZW and SZD dimensions from the fractographic images of ductile fracture surfaces has been developed.

10.2.1 Stretch Zone Analysis

10.2.1.0: Image Analysis Techniques

To measure the stretch zone using image analysis technique, a code has been developed in Visual C++, which can read bitmap image files of fractographs obtained from SEM. As the edges of the SZ are often not very prominent from the signals obtained from the original fractograph, various image enhancement algorithms have been implemented to bring out the desired features prominently.

Image enhancement approaches can be broadly divided in two categories [7]: Spatial domain methods and the frequency domain methods. Spatial domain refers to the image plane itself; approaches in this category are based on the direct manipulation of the image pixels. On the other hand, frequency domain method is based on modifying the Fourier transform of the image. All the algorithms in the code for image enhancement have been implemented using spatial domain methods.

A spatial domain method can be expressed by the simple expression [8]

$$g(x, y) = Tf(x, y) \quad \dots \text{eq 10}$$

where, $f(x, y)$ is the input image, $g(x, y)$ is the output image and T is an operator on f defined over some neighbourhood of (x, y) . A neighbourhood about (x, y) is defined by using a quadratic square or rectangular sub-image area centred at (x, y) . The centre of the sub-image is moved from pixel to pixel covering the entire image area and for each position of (x, y) , the operator T is applied to get a new value g at that point. The sub-image may be called by various names such as filter, mask, kernel, template or window. Figure 17 shows transformation of the original fractograph by using four enhancement and edge detection algorithms such as Histogram Equalisation, Laplacian filter, Sobel filter and Kirsch filter.

10.2.1.1. Automatic thresholding

The most common way of converting grey scale image to binary image is by *discrimination* or *thresholding*. Thresholding need not be done on the original grey scale image. The image processing operations can be used to alter the original brightness values such that make it is easier to select threshold values for the discrimination that will successfully separate any object from its background.

Manual setting of thresholds is most often accomplished interactively in standard image analysis software and it is the user's responsibility to select appropriate threshold values to delineate the features of interest. Error in such threshold settings is liable to cause bias in the measured parameters. For instance, if the manual threshold is set lower than the actual threshold value then the size of the object will be reduced. Using the same settings on different images from the same or similar samples may not be appropriate if the overall brightness level or contrast changes, or if the sample preparation is different. This can be a major source of error in the final results.

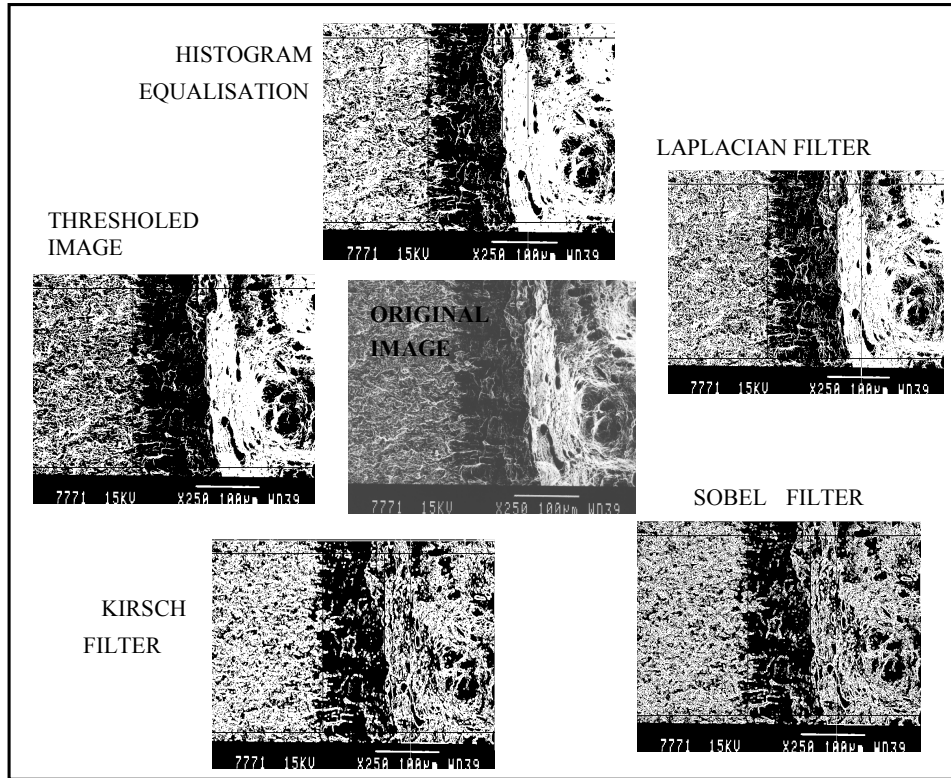


Figure 17 : Processed images of the original fractograph by using four enhancement techniques

Based on a heuristic approach an automatic thresholding [8] has been used which rely on the inspection of the histogram and on initial estimate of threshold value T_0 . This value gets refined by computing a new threshold, T_i , from the average grey level values of the segmented image obtained from the previous threshold T_{i-1} , through successive iterations.

This automatic thresholding worked well with the images containing SZW features. Since there is no option for selecting the threshold manually, the SZW is reproducible for the specified edge detection filter.

Figure 18 shows the average image signal before binarisation, Figure 14(b) shows the image signal after binarisation and Figure 14 (c) shows the processed image indicating the spatial correlation of the SZW feature with the signals obtained in Figures 14 (a) and 14 (b).

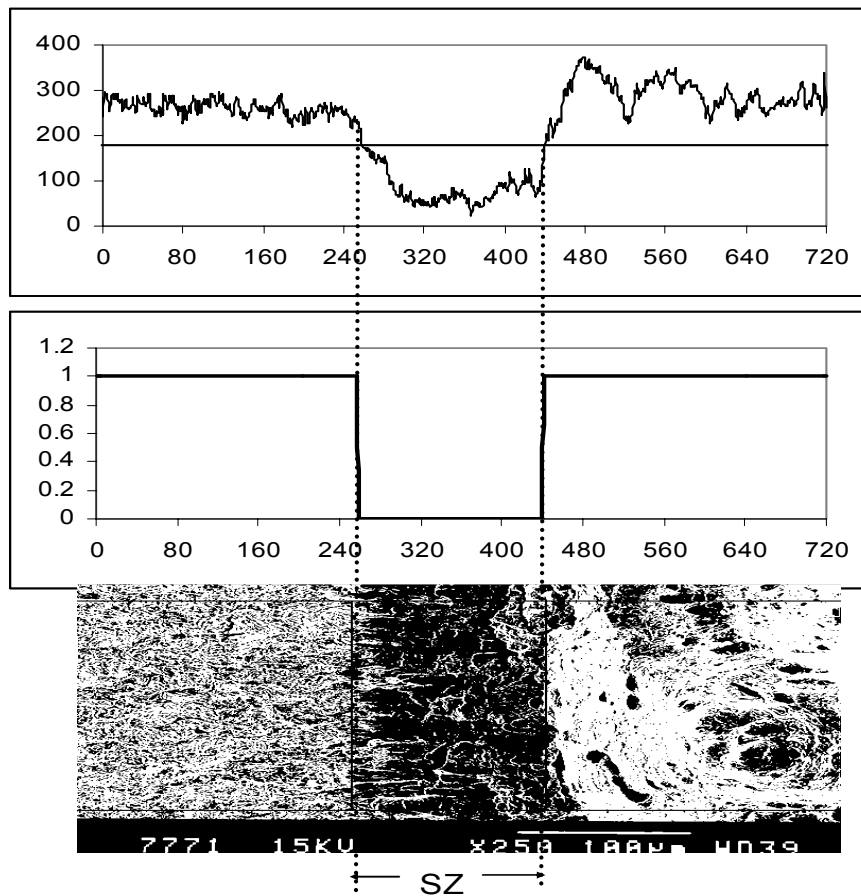


Figure 18 (a) Average image signal before binarisation
 (b) Image signal after binarisation
 (c) Processed SEM image of the fracture surface where the signals
 obtained in (a) and (b) are correlated with the image by two vertical lines

10.2.1.1 Stretch Zone Analysis by Image Processing

In ductile materials, crack will first blunt, extend virtually and then grow in a stable manner. Virtual crack extension, prior to stable tearing, in ductile materials leaves a signature in the form of the SZ. It is a region between the end of the fatigue pre-crack front and the onset of ductile tearing. Figure 19 (a) shows the schematic elevation profile of the crack-tip zone in a fractured specimen. Figure 19 (b) shows the SEM image of the fracture surface. The spatial correlation between the fractograph and the schematic representation of the crack tip zone can be seen very clearly.

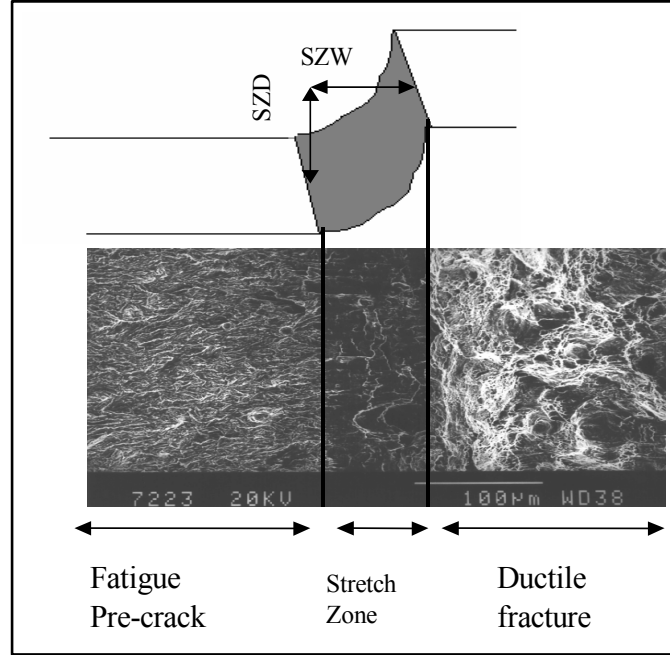


Figure 19 (a) Schematic elevation profile of crack tip zone
 (b) SEM image of the fracture surface

The aforementioned image/edge-enhancement techniques have been employed here to enhance boundaries of the stretch zone. The automatic thresholding algorithm [8] is used for segmentation and feature extraction. For the measurement of the width of the SZ, the pixels are calibrated automatically using the micron marker on the fractographs. The width of the stretch zone is computed as

$$SZW_{IA} = \chi \cdot w \quad \dots \text{Eq 10}$$

where χ is the conversion factor from pixel to length unit and w is the number of pixels contained within the width of the stretch zone.

The stretch zone depth (SZD_{IA}) can be estimated from a pair of fractographs, one taken from a 45° tilted specimen and the other taken on the same specimen without tilt. The SZ measured from the tilted specimen, it is denoted by SZT. Sivaprasad et. al [9,10] have devised a correlation to compute SZD as

$$SZD = \sqrt{2} \cdot SZT - SZW \quad \dots \text{Eq 11}$$

Eq. 11 is a special case when the tilt angle is 45° . For any tilt angle, α , correlation becomes

$$SZD = \frac{SZT - SZW \cos \alpha}{\sin \alpha} \quad \dots \text{Eq 12}$$

It may be noted that the error in computing SZD using the above correlation depends on the accuracy in identification of the true plane of fracture. The stretch zone width and depth measured by IA method is referred SZW_{IA} and SZD_{IA} respectively.

10.2.1.2 Manual Estimation of Stretch Zone dimensions

The pre-requisite to apply the proposed technique is the generation of ductile fracture surfaces. The fracture surfaces, carefully extracted from the broken halves of the tested specimens were examined in the SEM. Stretch zone features were recorded without tilting the specimen at sufficiently high magnification so that the whole width of the stretch zone was contained within the field of view. Then the specimen was tilted to 45 degree in the SEM stage and the stretch zone was recorded at the same magnification. While tilting specimen, care was taken to ensure that there was no lateral shift of specimen, so that the same area of fracture surface examined earlier was being viewed. Care was taken to ensure that a good contrast was obtained, so that the stretch zone limits could be demarcated easily. Approximately 30 measurements were made manually from each microphotograph recorded along the thickness direction on both halves of the specimens. In fact, the SZW measurement method documented in JSME S001 procedure [11] recommends a three point average of SZW at the mid-thickness of the specimen. In the present investigation, more number of measurements were made (along 2mm in the mid-section of the specimen) so that a meaningful statistical average could be obtained. Using the stretch zone width (SZW) obtained from the untilted image and its projection (SZT), the stretch zone depth (SZD) measurements were calculated employing eqn. 10. The mean values of these measurements obtained for each prestrained condition were taken to be representative of that condition. Visual examination of fracture surface revealed that the stretch zone was apparently uniform in the mid-thickness of the specimen. However, when the stretch zone dimensions were measured, it was noted that the magnitudes of SZW, SZT and that of SZD varied across the specimen thickness. A typical variation of SZW, SZT and SZD across the specimen thickness is shown in Figure 20. Scatter in SZW measurements has been statistically analysed by a round robin programme organised by the European Group of Fracture [12]. It is brought out clearly that the subjectivity in defining the stretch zone boundary can give rise to high scatter and proposes such measurements to be carried out by persons with good working experience in SEM in order to have minimum error.

The stretch zone width and depth measured by manual method is referred SZW_{man} and SZD_{man} respectively.

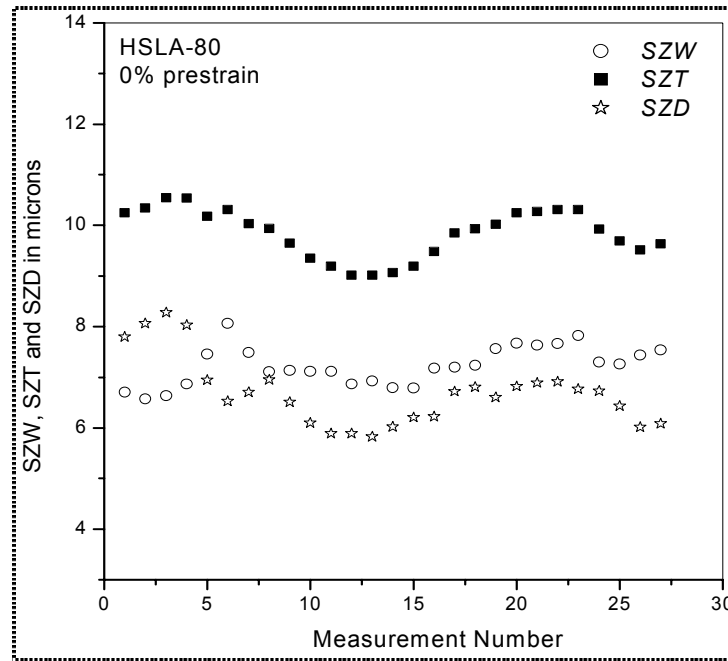


Figure 20: A typical variation in measured SZW, SZT and SZD values across the specimen thickness obtained by manual measurement

10.2.1.3 Stretch zone dimensions from fracture resistance curve

From the initiation fracture toughness, J_i , stretch zone width can be determined using the blunting line equation:

$$J_i = M\sigma_0 \Delta a_{cr} \quad \dots \text{Eq 13}$$

where σ_0 is the flow stress of the material and Δa_{cr} is the critical virtual crack extension prior to the onset of ductile tearing which is equivalent to stretch zone width.

Through standard plain strain fracture toughness testing, J_i is computed at the intersection of the blunting line and the power law curve fitted for the non linear portion of the J - Δa data as mentioned earlier. Substituting the value of J_i in the Eq. (13) and for the known blunting line slope, M , the SZW_R is estimated.

For the determination of SZD_R , we have used δ - Δa curve from which critical δ_c is computed. Half of the δ_c is the value for SZD_R .

The stretch zone width and depth measured indirectly via fracture resistance curve is referred SZW_R and SZD_R respectively.

10.2.2 Crack tip profile estimated by IA and J-R curve method

In order to study the variation of the crack tip profile, a HSLA steel was variously prestrained at 0%, 1%, 2%, 3% and 5% to arrive at different strength-toughness properties. Stretch zone analysis of the fracture surface has been performed to obtain the SZW and SZD values. It may be reiterated that SZW is the crack extension da and SZD is half of the CTOD. For a semicircular crack tip profile $SZW=SZD$. Figure 21 shows the crack tip profile by the IA and J-R curve methods. It is interesting to note that the crack tip profile obtained from the J-R curve predicts that the material has strain hardening property, n , more than 0.3, whereas it is below 0.2 as predicted by the IA method. These strain hardening values have been obtained using Figure 14 (a) for the estimated crack tip profile parameter, X . It is interesting to note that the material has n value less than 0.2 as obtained by the tensile tests.

It may be noted that for estimation of stretch zone dimension from fracture resistance data, a blunting line is constructed as per ASTM standard for the $J-da$ data points falling within the window of $0.2 J_i$ to $0.6 J_i$. The slope of this blunting line and J_i thus determined are then used to compute the magnitude of stretch zone dimension. Referring to Figure 21, the diagonal line represents the locus of $SZW=SZD$ for a semicircular crack tip profile. The data points below this line represent a positive deviation from semicircular crack tip profile and those above this line indicate a negative deviation as schematically depicted.

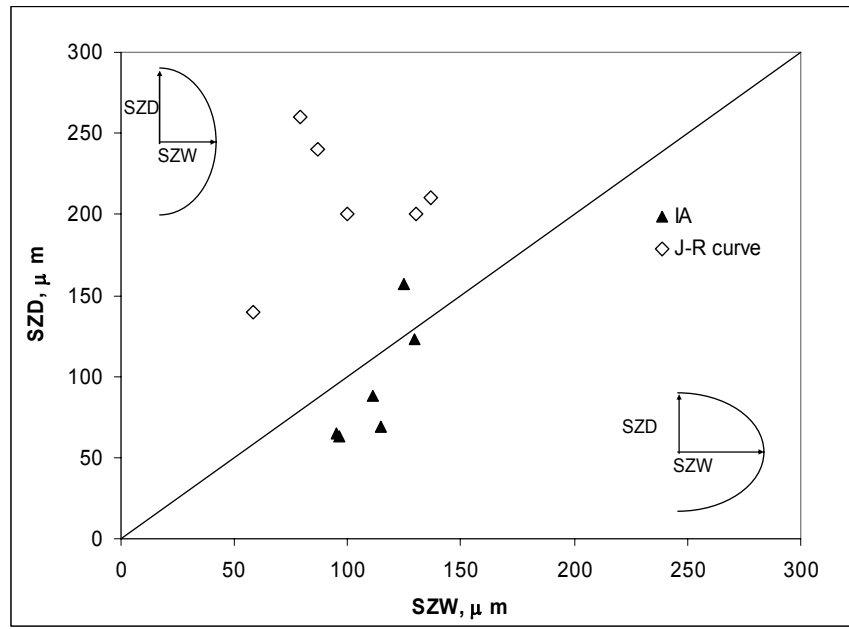


Figure 21: Co-relation between SZW and SZD showing the crack tip profile

It may be noted that the stretch zone dimension data obtained by image analysis technique fall below the diagonal line whereas those derived from the fracture resistance curve fall above this line. If the fracture surface is believed to keep a more representative imprint of crack tip blunting process, then the larger SZW dimensions by image analysis technique indicates that the crack tip has experienced extensive stretching resulting in larger physical crack extension. In fact, this is quite common in high toughness materials such as HSLA steels [14]. This extensive stretching could not be accounted for when SZW_R is determined from the fracture resistance data. This may be due to the narrow data range that has been considered for constructing the blunting line as suggested in the ASTM standard. Perhaps, the narrow data range is insufficient to portray the crack tip blunting process completely resulting in inaccurate estimations of J_i and hence SZW_R . In such high toughness materials, a higher data range should therefore be considered for drawing a blunting line. At the same time, the dominance of the strain controlled fracture mechanism [13], predominantly observed in upper bound data range (i.e. $0.2 J_i$ to $0.9 J_i$) incorporates unusually a higher degree of non-linearity in blunting line [14] in this grade of steel. Selection of appropriate data range for computing the blunting line slopes remains to be a point for further investigation.

In order to investigate the influence of increased blunting line data range on SZW, various upper bound data windows were considered for estimating the blunting line and

subsequently SZW_R values are computed. Figure 22 shows a comparison of SZW_R calculated from various data ranges and SZW_{IA} . It can be seen that a reasonable agreement with SZW_{IA} is obtained when SZW_R values are calculated using 0.2 J_i to 0.8 J_i data range for constructing the blunting line. It appears, therefore, in high toughness materials a judicious selection of data range for blunting line is necessary for determination of J_i and SZW .

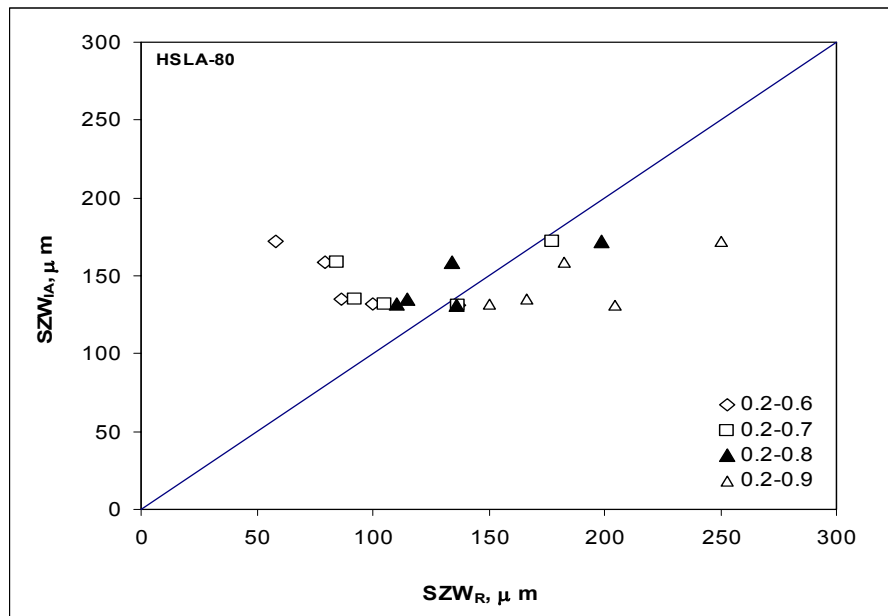


Figure 22: SZW_{IA} and SZW_R for various data ranges.

Crack tip profile estimated by direct observation using CCD camera

For on-line monitoring and estimation of the crack tip profile, a device called “Real time Optical cracktip Monitoring System (ROMS)” has been used. The device has very high resolution CCD camera, illumination system, image capturing cards and software and a laptop for storing image data. A set of images captured using the system for 304Ln steel is shown in Figure 23. The images show how the crack tip blunts during the monotonically increasing loading process. At certain stage two sharp corners are visible; one of which extend more than the other showing the direction of crack propagation. For the estimation of the crack tip profile, the CTOD has to be estimated. Since the location for the CTOD measurement is a point of debate, we need to look into it in great details. The estimation of the crack tip profiles remains to be the future research endeavour.

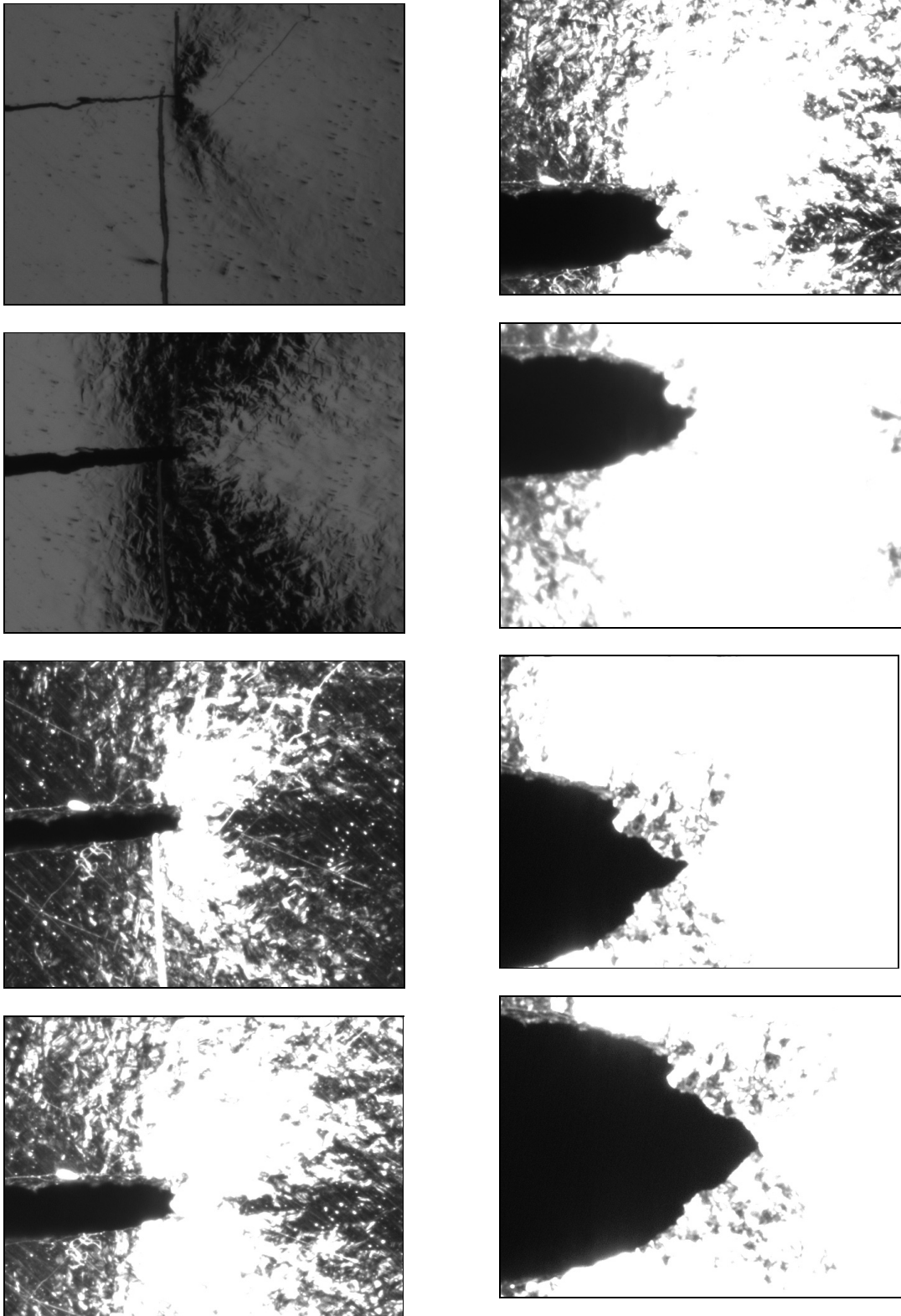


Figure 23: A set of images captured by ROMS showing the crack tip blunting

11. Conclusions

From the numerical study conducted for simulating crack tip blunting behaviour in ductile materials, the following could be concluded:

- ◆ the blunting line is non-linear, contrarily to the assumption that it is linear. FE analysis of the HSLA-100, TLXAL and SA333 materials confirmed this.
- ◆ the blunting line is mildly sensitive to the level of flow stress, with the inflection occurring at a lower flow stress and with reduced sharpness as the flow stress is increased. The blunting line slope is higher in low strength materials.
- ◆ the nature of the blunting line is greatly dependent with the work hardening capacity of the material, with the overall slope of the blunting line increases with increased hardening behaviour.
- ◆ the crack tip profile was found to be elliptical not semicircular. For the low strain hardening materials the crack tip profile parameter, $X=CTOD/da$ is less than 2 whereas for the high strain hardening materials it is more than 2.
- ◆ An image analysis technique proposed in this investigation to estimate the crack tip profile through the measurement of stretch zone width (SZW) and stretch zone depth (SZD) enhances the quality of the fractographic images and thus improves the accuracy of the measurement and minimises the subjectivity in identifying the stretch zone boundaries.
- ◆ Stretch zone dimensions in a high toughness HSLA steel has been estimated at various prestrain levels using this technique and the results are compared with those obtained from manual measurements and from fracture resistance data. A good agreement is noted between the image analysis and manual methods. In case of stretch zone dimensions from fracture resistance data, it is noted that the data range ($0.2 J_Q$ to $0.6 J_Q$) suggested in the ASTM standard for constructing the blunting line is insufficient and this caused inaccuracy in measurements. When the data range is increased to $0.2J_Q$ to $0.8J_Q$, a reasonable agreement in stretch zone dimensions by all the methods is observed.
- ◆ The crack tip profile obtained by the stretch zone analysis method confirms the blunting line slope predicted by the FE analysis of low strain hardening materials.
- ◆ A software package has been developed using the proposed image analysis technique to measure the stretch zone dimensions. This software, apart from giving the stretch zone dimensions from fractographic images, will also automatically compute the J_i , J_Q and J_{IC} values both using the stretch zone dimension data and following the ASTM

standard. Provision to select a user defined data range to construct the blunting line has also been incorporated in the software.

References

1. ABAQUS 6.4 : ABAQUS Engineering Analysis Solutions (Pvt.) Ltd, India, abaqus@abaqus.co.in
2. [E 1152-96], Test Method for Determining J-R Curves, ASTM STP Annual Book of ASTM Standards, ASTM, Philadelphia, PA, 03.01 (1996)
3. T. R. Chandrupatla and A.D. Belegundu: 'Introduction to Finite Element in Engineering', Prentice Hall of India Pvt. Ltd. India (1991)
4. [E 1737-96], Standard Test Method for J Integral Characterisation of Fracture Toughness, ASTM STP Annual Book of ASTM Standards, ASTM, Philadelphia, PA, 03.01 (1996) 968
5. G. E. Dieter: 'Mechanical Metallurgy Second Edition,' Mcgraw-Hill Kogakusha Ltd., 1976
6. M. F. Kanninen and C. H. Popelar: 'Advanced Fracture Mechanics,' Oxford University Press, New York, 1985
7. John C. Russ: Computer Assisted Microscopy, Plenum Press, New York (1990)
8. Rafael C. Gonzalez, Richard E. Woods: 'Digital Image Processing' 2nd Edition Pearson Education (Singapore) Pvt Ltd. India (2002)
9. S. Sivaprasad, S. Tarafder, V. R. Ranganath, S. K. Das, K. K. Ray: Met. Metallurgical and Materials Transactions, 33A (2002) 3731
10. S. Sivaprasad, S. Tarafder, V. R. Ranganath, K. K. Ray: J. Mater. Sci. Eng. A284 (2000) 195.
11. H. Kobayashi, H. Nakamura, H. Nakazawa, Elastic-Plastic Fracture: Second Symposium, Volume II-Fracture Resistance Curves and Engineering Applications, ASTM STP 803, C.F. Shih and J. P. Gudas, Eds., American Society for Testing and Materials,(1983) II-420
12. ESIS P2-92, ESIS procedure for determining the fracture behaviour of materials, Technical Committee I: Elastic-Plastic Fracture Subcommittee 1.4: Fracture Mechanics Testing Standards (1992)
13. R. J. Barnhurst, J. E. Gruzleski: Metall. Trans. 16A (1985) 613.
12. K. Ohji, A. Otsuka, H. Kobayashi: Elastic-Plastic Fracture: Second Symposium, Volume II-Fracture Resistance Curves and Engineering Applications, ASTM STP 803, C.F. Shih and J. P. Gudas, Eds., American Society for Testing and Materials,(1983)II-398

APPENDIX-I

Dimensions of the specimen geometry

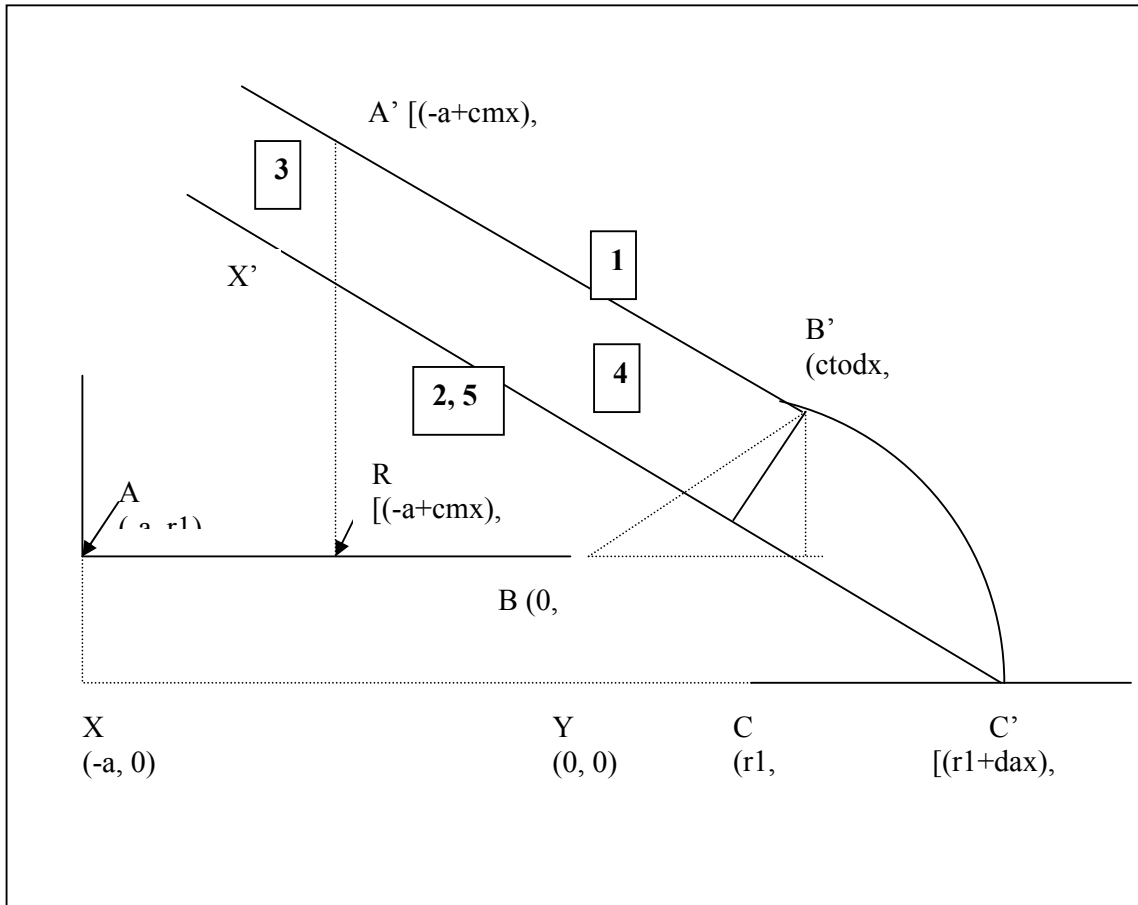
Materials	Specimen Type	Crack length, a	Width, W	Thickness, B	Net thickness (after sidegrooving) B_n
HSLA-80, 0%PS*	TPB	10	19.79	4.33	4.33
HSLA-80, 1%PS*	TPB	10	19.773	4.313	4.313
HSLA-80, 2%PS*	TPB	9.291	19.593	4.2933	4.2933
HSLA-80, 3%PS*	TPB	10	19.587	4.327	4.327
HSLA100	TPB	18.065	29.85	19.55	15.8
HSLA-100(T=350)	TPB	21.92	30.11	20.02	15.98
HSLA-100(T=700)	TPB	18.15	30.04	20.03	15.12
HSLA-100(T=650)	TPB	17.60	30.01	20.06	15.12
HSLA-100(T=550)	TPB	19.97	30.12	20.03	15.06
HSLA-100(T=600)	TPB	19.98	30.18	20.13	16.04
TLXAL	TPB	15.01859	29.98	12.7	12.7
SA333	TPB	12.5	25	12.66	10.48
LN304SS	CT	13.4	25.025	8.03	8.03

PS= Pre strained

Material Properties and the blunting line slopes

Materials	Young's Modulus (MPa)	Strain hardening	Yield Stress (MPa)	Ultimate Tensile Stress (MPa)	Fracture Stress (MPa)	Fracture strain	M_FEM	M_exp
HSLA-80, 0%PS*	201781	0.11	637	708.00	376.00	0.24	2.70	6.2
HSLA-80, 1%PS*	1958560	0.09	658	723.51	382.93	0.21	2.60	6.9
HSLA-80, 2%PS*	191512	0.07	672	724.79	399.26	0.19	2.50	7.9
HSLA-80, 3%PS*	191827	0.06	700	734.61	403.56	0.19	2.50	3.8
HSLA100	195000	0.06	818	1004	392	0.211	2.16	2.4
HSLA-100(T=350)	203300	0.06	886	1056	460	0.22	2.16	2.3
HSLA-100(T=700)	194000	0.08	831	983	603	0.25	2.4	2.2
HSLA-100(T=650)	175400	0.14	640	921	560	0.20	2.4	1.4
HSLA-100(T=550)	192700	0.16	927	1011	626	0.31	2.4	1.4
HSLA-100(T=600)	187700	0.19	698	955	549	0.13	2.6	1.6
TLXAL	190000	0.15	470	582.76	437.29	0.29	2.60	3.3
SA333	188990	0.22	295	463	235	0.3	5.0	4.74
304LN	190000	0.25	289	682.87	346.09	0.70	12.00	11.6

Techniques for the calculation of Δa



Crack tip region for computing virtual crack extension

r_l (root radius) = 0.02 mm

cmx, cmy=crack mouth opening displacements

ctodx, ctody=crack tip opening displacements

dax, day= crack tip displacements

- ◆ The (x, y) co-ordinates of A', B' and C' are obtained by FEM, where

$$A': [(-a+cmx), (r_1+cmx)]$$

$$B': [ctodx, (r_1+ctody)]$$

$$C': [(r_1+dax), 0]$$

1. Equation of the straight line passing through A'B'.

Equation of straight line: $y = m_1x + c_1$.

First we require to calculate the slope of A' B' using the expression:

Slope $m_1 = \frac{y_2 - y_1}{x_2 - x_1}$, for A' (x_1, y_1) and B' (x_2, y_2)

$$m_1 = \frac{(r_1 + ctody) - (r_1 + cmy)}{(ctodx) - (-a + cmx)} = \frac{ctody - cmy}{a + ctodx - cmx}$$

Next get the intercept of the straight line A'B'. For this, either the values of x_1 and y_1 and slope m in the eqn of straight line $y=mx+c$, or the values of (x_1, y_1) and (x_2, y_2) are substituted in the expression: $c_1 = \frac{x_2 y_1 - x_1 y_2}{x_2 - x_1}$.

2. Equation of straight line parallel to the above line A'B' and passing through C'.

We know that the slopes of two parallel lines are same. The line parallel to A'B' is X'C' as can be seen from the figure above. Slope of the line is m_1 , we require to get the intercept of the line X'C', which is c_2 .

$$y = m_1 x + c_2 \Rightarrow c_2 = y - m_1 x \text{ where } x, y \text{ are the co-ordinates of point C'}$$

$$c_2 = 0 - m_1(r_1 + dax).$$

3. A'X'- the perpendicular distance of A' to the line X'C'

The perpendicular distance from the point (x_1, y_1) to the line $y = mx + c$ is given by the expression: $\frac{|y_1 - mx_1 - c|}{\sqrt{m^2 + 1}}$,

where A' (x_1, y_1) and eqn of line X'C' is $y=m_1x+c_2$

$$\text{Perpendicular distance A'X'} = \frac{|(r_1 + cmy) - m_1(-a + cmx) - c_2|}{\sqrt{m_1^2 + 1}}.$$

4. Length of A'C'

If (x_1, y_1) and (x_2, y_2) are points on the line whose equation is $y=mx+c$, then the distance between them is: $|x_2 - x_1|\sqrt{m^2 + 1}$,

Where A'(x_1, y_1) and C'(x_2, y_2).

$$\text{Distance A'C'} = |(r_1 + dax) - (-a + cmx)|\sqrt{m_1^2 + 1}.$$

5. Length of X'C'

Once the distances A'X' and A'C' are known, then we can calculate

$$X'C' = \sqrt{(A'C')^2 - (A'X')^2}.$$

6. Calculation of Δa

$$\Delta a = X'C' - (a + r_1)$$

Determination of δ_t (CTOD) from FEM analysis

1. Get FEM data in this order: *Load steps, RF, cm_x, dax, ctod_x, cm_y, day, ctod_y*. Here the letters ‘x’ and ‘y’ signify the respective displacements in the x and y directions. The definitions of the parameters are the following

RF=Reaction force subjected to half of the model
cm_x, cm_y=Crack mouth opening displacement along x and y directions
da_x, da_y=Crack tip displacement along x and y directions
Ctod_x, ctod_y=Crack tip opening displacement along x and y directions

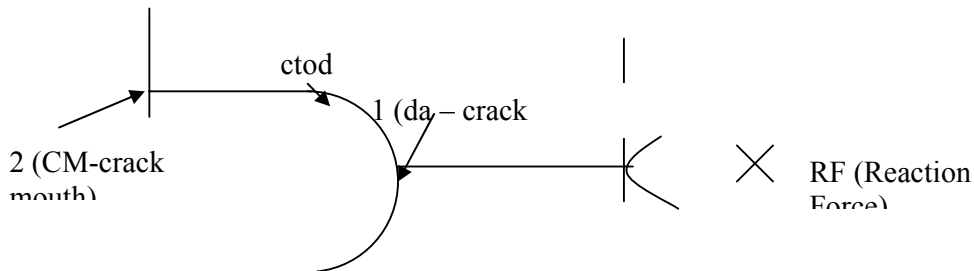
2. The applied load is calculated using $load = \frac{-2 \times RF}{conversion}$. At the time of doing the analysis, if Young’s modulus and yield stress are given in MPa and the displacements in mm, then the load is obtained in Newton (MPa = N/mm²). Conversion factor can be taken as 10³ if the load is to be converted to kN.
3. Displacement is calculated: $Displacement = 2 \times cm_y$. As all lengths are given in mm during the analysis, so the displacement is obtained in mm.
4. Δa is obtained using the technique described in appendix-I.
5. The inverse of elastic slope is calculated as follows:

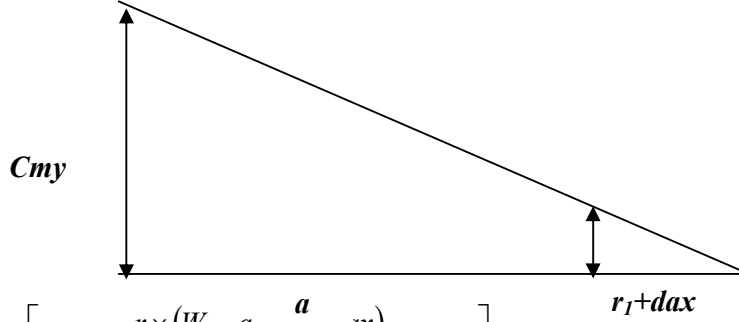
$$C_{cm(i)} = \frac{S}{E' \times B_e \times W} \times 6 \times \left(\frac{a_i}{W}\right) \times \left[0.76 - 2.28 \left(\frac{a_i}{W}\right) + 3.87 \left(\frac{a_i}{W}\right)^2 - 2.04 \left(\frac{a_i}{W}\right)^3 + \frac{0.66}{\left(1 - \frac{a_i}{W}\right)^2} \right]$$

where $a_i = (a + r1 + \Delta a)$, $\left(\frac{a_i}{W}\right) = \left(\frac{a + r1 + \Delta a}{W}\right)$ and $B_e = B_{effective} = B - \left(\frac{(B - B_n)^2}{B}\right)$

$$E' = \frac{E}{(1 - \nu^2)} \text{ for plane strain case}$$

6. $V_{cm_e} = load \times C_{ll(i)}$.
7. $V_{cm_p} = (displacement - V_{cm_e})$





8.
$$\delta_p = \left[\frac{r \times (W - a - r_1 - dax)}{(a + r_1 + dax) + (W - a - r_1 - dax) \times r} \right] \times V_{cm-p}$$
, where r is the rotational factor which is considered as 0.44 for a TPB specimen.

9. In order to calculate the stress intensity factor, the value of $F(a/W)$ is to be obtained. The expression $F(a/W)$ is written as (Numerator/Denominator). The numerator is calculated as follows:

$$(3 \times \sqrt{a_w}) \times (1.99 - a_w \times (1 - a_w) \times (2.15 - 3.93 \times a_w + 2.7 \times (a_w)^2)), \quad \text{where } 'a_w' \text{ is}$$

obtained as follows:
$$a_w = \frac{a + r_1 + \Delta a}{W}$$

10. The denominator is obtained as follows: $2 \times \sqrt{1 - a_w} \times (1 - a_w) \times (1 + 2 \times a_w)$.

11. The stress intensity factor, $K = \frac{S \times load}{\sqrt{W} \times W} \times F\left(\frac{a}{W}\right)$, where S ($4 \times W$) is the length of the span.

12. The elastic component of CTOD is calculated as follows:

- For plane strain: $\delta_e = \frac{K^2(1 - \nu^2)}{2 \times \sigma_{ys} \times E}$ and
- For plane stress: $\delta_e = \frac{K^2}{2 \times \sigma_{ys} \times E}$.

13. The total CTOD is calculated: $\delta_t = \delta_e + \delta_p$.

Experimental Data

In the experimental load displacement data, the load component is divided by $B_{effective}$, i.e. load/ $B_{effective}$, which is obtained by using B (specimen thickness) and B_n (specimen thickness without notch).

$$B_{effective} = \sqrt{(B \times B_n)}$$

Consistency of Units

N.B: When analysis is done using ABAQUS, we are supplying all the values in MPa (N/mm^2), i.e the Young's Modulus in MPa (eg: for 100Gpa, we give it in MPa as 100e3), the yield stress in MPa (eg: 300MPa as 300).

When carrying out the data analysis using the software, the load calculation is done using a conversion factor of 1000, in order to get the load value in kN; load = (-2 X RF)/1000.

$$MPa = \frac{N}{mm^2}$$

$$MPa \times 10^{-3} = \frac{N \times 10^{-3}}{mm^2}$$

$$GPa = \frac{kN}{mm^2}$$

As we are converting the load in kN, therefore we require to give the values of Young's Modulus and yield stress in GPa, and all length units in mm.